Surveys in Geophysics (2019) 40:881–911
https://doi.org/10.1007/s10712-019-09532-0

Upscaling Forest Biomass from Field to Satellite Measurements: Sources of Errors and Ways to Reduce Them

Maxime Réjou-Méchain[1] · Nicolas Barbier[1] · Pierre Couteron[1] · Pierre Ploton[1] · Grégoire Vincent[1] · Martin Herold[2] · Stéphane Mermoz[3,8] · Sassan Saatchi[4] · Jérôme Chave[5] · Florian de Boissieu[6] · Jean-Baptiste Féret[6] · Stéphane Momo Takoudjou[1,7] · Raphaël Pélissier[1]

Received: 16 October 2018 / Accepted: 12 April 2019 / Published online: 30 May 2019

Abstract
Forest biomass monitoring is at the core of the research agenda due to the critical importance of forest dynamics in the carbon cycle. However, forest biomass is never directly measured; thus, upscaling it from trees to stand or larger scales (e.g., countries, regions) relies on a series of statistical models that may propagate large errors. Here, we review the main steps usually adopted in forest aboveground biomass mapping, highlighting the major challenges and perspectives. We show that there is room for improvement along the scaling-up chain from field data collection to satellite-based large-scale mapping, which should lead to the adoption of effective practices to better control the propagation of errors. We specifically illustrate how the increasing use of emerging technologies to collect massive amounts of high-quality data may significantly improve the accuracy of forest carbon maps. Furthermore, we discuss how sources of spatially structured biases that directly propagate into remote sensing models need to be better identified and accounted for when extrapolating forest carbon estimates, e.g., through a stratification design. We finally discuss the increasing realism of 3D simulated stands, which, through radiative transfer modelling, may contribute to a better understanding of remote sensing signals and open avenues for the direct calibration of large-scale products, thereby circumventing several current difficulties.

Keywords Biomass · Calibration · Carbon · Error propagation · Field data · Modelling

1 Introduction

The large uncertainty associated with the global spatio-temporal dynamics of forest carbon (C) is a major obstacle to the projection of future atmospheric CO_2 concentrations and the implementation of mitigation strategies. Satellite observations of land-use changes are currently reliable enough to provide robust information on deforestation dynamics (Hansen

✉ Maxime Réjou-Méchain
maxime.rejou@ird.fr

Extended author information available on the last page of the article

et al. 2013). However, the associated C release remains uncertain because broad-scale C mapping applications from satellite data still convey large uncertainty (Mitchard et al. 2013; Huang et al. 2015; Rodriguez-Veiga et al. 2017). Even higher uncertainty is associated with C fluxes related to forest degradation and regrowth because small changes in the C stocks in closed-canopy forests are challenging to detect remotely (Bustamante et al. 2016), resulting in an underestimation of forest degradation globally (Pearson et al. 2017).

Forest aboveground biomass (AGB), the main proxy for forest C stock, is rarely directly measured, either in the field or via remote sensing (RS) (Clark and Kellner 2012). AGB estimations are thus derived from statistical models with their own underlying assumptions that can generate random and/or systematic errors when violated. The way the errors that are associated with these models propagate up to the final AGB estimate is, however, generally poorly understood and accounted for. A simple illustration of how RS–AGB models may produce inaccurate AGB density maps is shown in Fig. 1. First, the propagation of a uniform bias over calibration data (e.g., field plot AGB estimates) conveys a systematic over- or underestimation, which may be straightforward to correct in the final density map provided that the bias can be quantified (Fig. 1b). A more overlooked but common effect is the propagation of a non-uniform bias, leading the RS model to overestimate small AGB values and underestimate large AGB values, resulting in density maps flattened around the mean (Fig. 1c; Avitabile et al. 2016; Xu et al. 2016). Such bias may originate from three sources: (1) a non-uniform bias exists in the calibration dataset, such as an AGB over- or underestimation in young versus old successional forests, which can be corrected if the non-uniform pattern of errors is well identified a priori; (2) the low sensitivity of RS signals to high AGB values generally results in an AGB underestimation (i.e. signal saturation), while in low AGB open areas, non-forest land surfaces (i.e. surface roughness, non-woody vegetation) also contribute to the remotely sensed signal, leading to an overestimation of forest AGB; (3) in regression models, violation of the assumption of low/non-existent error in the independent variable (the "observed" AGB) results in a systematic underestimation of the model slope (Fuller 1987; Réjou-Méchain et al. 2014). Finally, the major source of

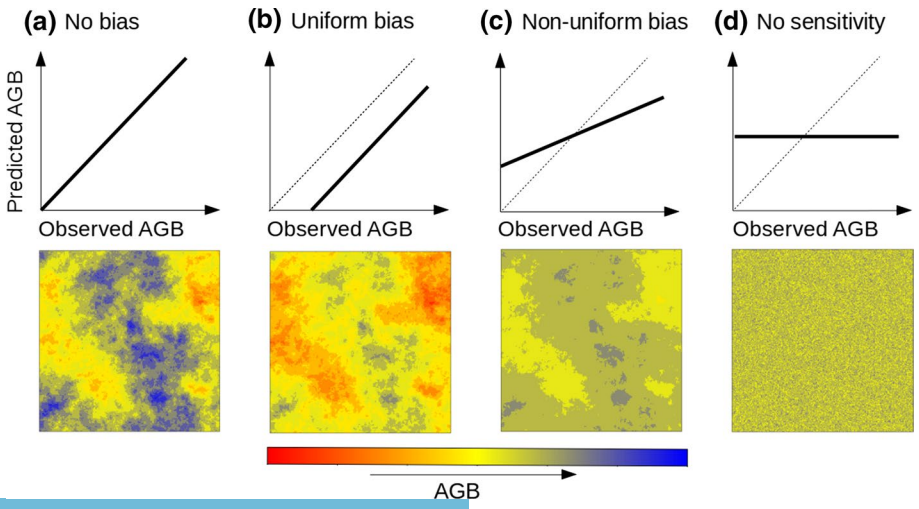

Fig. 1 Conceptual representation of common bias patterns found in remote sensing AGB models

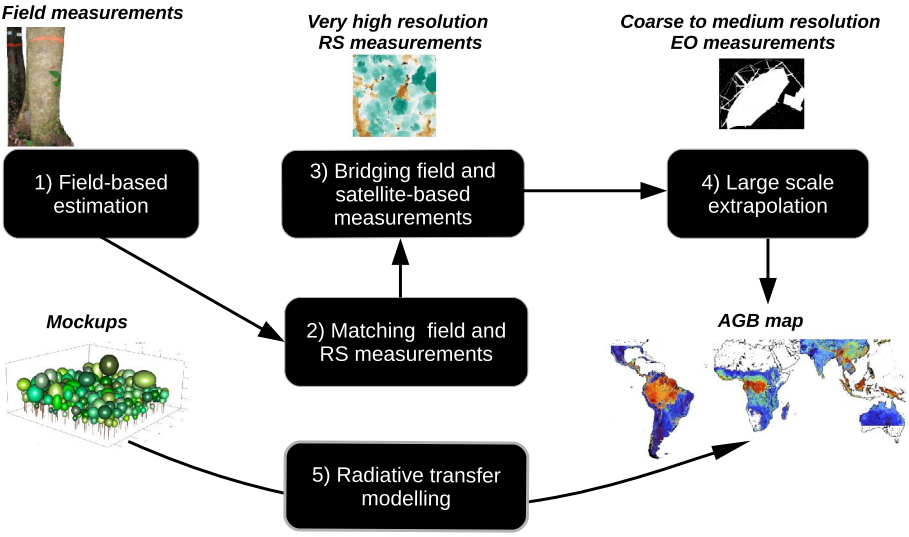

Fig. 2 Flowchart illustrating the main sections of this paper

uncertainty in RS-based models is obviously the poor signal sensitivity to AGB variations, which makes the post-correction of density maps impossible (Fig. 1d).

In this paper, we review the sources of errors that may occur during the process of upscaling AGB estimates from ground to RS data and provide suggestions for reducing these errors (Fig. 2). Section 2 illustrates that field-based estimates—often improperly seen as "ground truth"—most likely convey more important errors than generally assumed. Section 3 discusses the issues associated with mismatching field-based AGB estimates to RS data. Section 4 presents a multi-step calibration strategy aimed at bridging field and satellite measurements through airborne or spaceborne very high-resolution RS products. This section also highlights the pitfalls and promises of such a strategy. Section 5 discusses the common problems associated with broad-scale AGB extrapolations for regional mapping through inexpensive satellite imagery. Finally, Sect. 6 reviews physical modelling approaches and discusses how they may improve our ability to map AGB. These sections mostly focus on tropical forest examples, where uncertainty in C dynamics is the highest globally (Mitchard 2018), although most of the issues that are discussed are also concerns in other forest biomes.

2 Improving Field-Based AGB Estimation

Uncertainty in field-based AGB estimation has recently become a matter of concern for the RS community (e.g., Mermoz et al. 2014, 2015; Longo et al. 2016; Xu et al. 2017; Bouvet et al. 2018; Jucker et al. 2018a). For instance, Chen et al. (2015) developed an analytical framework to track the sources of errors from field measurements in airborne LiDAR-AGB predictions. The authors estimated that field-based uncertainty contributed only 10% of the total pixel-level uncertainty at a 0.16-ha resolution (see also Longo et al. 2016). However, the statistical framework developed by these authors rested upon the assumption that tree-level AGB estimation errors are independent within and between field plots; thus,

they average out in RS models. While this assumption is common (e.g., Chave et al. 2004; McRoberts and Westfall 2013; Longo et al. 2016), it is often violated, generating overlooked biases in AGB maps.

Field-based AGB estimates at the plot level are obtained by summing individual AGB values for all trees within the plot. At the tree level, AGB is generally estimated using an allometric model that combines key tree features, typically the stem diameter (D), total tree height (H) and wood density (WD; Chave et al. 2005, 2014). While D may suffer from important measurement errors (Clark 2002), significant efforts have been made towards protocol standardization (Phillips et al. 2009; Condit et al. 2014) to warrant negligible errors, at least in scientific plots (Chave et al. 2004; Molto et al. 2013). However, as shown below, the two other predictors, as well as the AGB model itself, may convey systematic error components within and between plots that may directly propagate into RS models.

2.1 Uncertainty in Wood Density

Individual tree AGB is directly proportional to WD, which varies by as much as tenfold among tree species (Chave et al. 2009). However, WD is rarely measured on individual trees in forest inventories, and in most cases, a mean specific value is assigned from independent databases to all trees of a given taxonomic category, often higher than the species level. This approximation is very crude beyond the genus level (Flores and Coomes 2011); however, it is common in the tropics because of inaccurate botanical identifications (Gomes et al. 2013) or the limited availability of WD data (Chave et al. 2009). For example, in the well-known pantropical forest inventory dataset generated by Al Gentry, which includes 43,000 trees (> 8000 taxa), more than one-third of the trees could not be assigned a WD value at the species or genus level from the Global Wood Density Database (Chave et al. 2009; Zanne et al. 2009). Given that most tropical tree taxa are spatially aggregated at various scales (Condit et al. 2000), uncertainty in WD estimates is expected to cause spatially structured errors, potentially generating biases in plot-level AGB estimates (Baker et al. 2004). One way to mitigate this error source is to rely on permanent scientific sites for model calibration. For instance, in the 50-ha Center for Tropical Forest Science (CTFS) permanent plot at Barro Colorado Island, Panama (Condit 1998), less than 2% of the trees have WD values assigned at a coarser taxonomic resolution than the genus level. In addition, repeated censuses also strongly minimize field measurement or encoding errors and reduce the number of missing trees (Lopez-Gonzalez et al. 2011), providing high-quality calibration data for RS applications (Chave et al. this issue).

The assignment of a WD value to an individual tree at the species level does not, however, ensure bias-free estimates. WD is known to vary widely between individuals of the same species and even within individual trees (Tarelkin et al. 2019; Swenson and Enquist 2008; Bastin et al. 2015a; Wassenberg et al. 2015). For example, species having at least 10 observations in the Global Wood Density Database ($n = 109$) exhibit a mean WD variation of 9% around the mean. Given that two-thirds of the taxa in that dataset are documented with a single measure, the effects of intra-specific variations in WD on AGB estimates are currently difficult to quantify. Intra-individual variations may also have a strong impact on field AGB estimations, e.g., when converting volume estimations (e.g., from terrestrial LiDAR, see below) into biomass. A recent study conducted in Cameroon showed a significant decrease in WD with height for most species; thus, the use of WD at the trunk base to convert volume into biomass led to an AGB overestimation of approximately 10% at

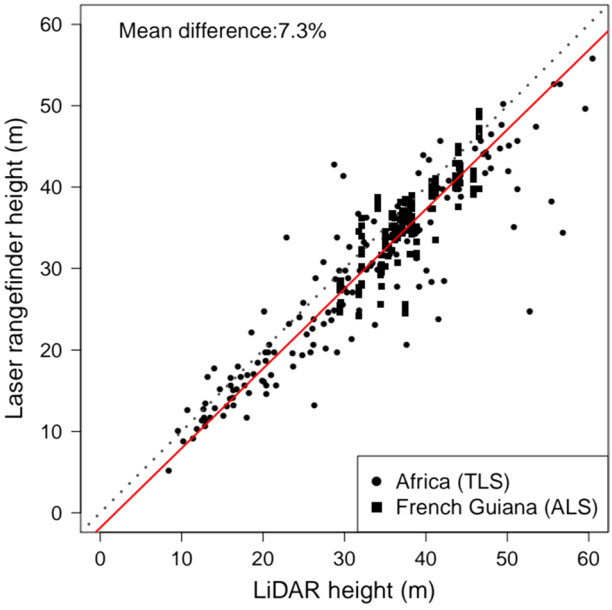

Fig. 3 Comparison between height measurements inferred from airborne or terrestrial LiDAR acquisitions and measured in the field using a laser hypsometer (TruPulse 360R for the 151 trees from Cameroon and Haglöf Laser Vertex for the 306 French Guiana trees). The relationship suggests that tree height measurements from laser rangefinders underestimate the tree height by 7.3%. The red line illustrates the output of a standard major axis regression (i.e. minimizing errors in both X and Y), and the dotted line represents the 1:1 line

the plot level (Sagang et al. 2018). The authors, however, demonstrated that vertical variations could be predicted from basal WD; thus, these variations could be controlled for in biomass estimations, which was recently confirmed in a large dataset from 6 different countries in central Africa (Momo Takoujdou et al. in preparation).

A lesson learned from this short review is that more efforts are needed to collect WD data for tropical taxa using standardized protocols (Williamson and Wiemann 2010) while accounting for all major sources of variation. Given the time and cost of wood core analyses, non-destructive and rapid WD measurement techniques are appealing, such as torsiometers, Pilodyns, nail withdrawal tools or emerging electronic devices to measure drilling resistance (reviewed in Gao et al. 2017). For instance, the use of an empirical model developed from Pilodyn measurements led to a predicted WD error of 15% for 1427 trees from four continents.

2.2 Uncertainty in Tree Height

As for WD, tree height is not systematically available from field plot inventories, and *H*–*D* models are often used to estimate the height (*H*) of individual trees from stem diameter (*D*) measurements. These models are built from *H* measurements that are subjected to errors, especially in dense forest canopies. Indeed, in addition to a strong operator effect, Larjavaara and Muller-Landau (2013) showed that the two most common *H* measurement methods (the so-called tangent method, which combines horizontal distance to the trunk and the angle to the treetop, and the "sine" method, which combines the angle and distance measurements to the treetop) led to significantly contrasting results, with an underestimation of ca. 20% with the "sine" method. Based on an original dataset of *H* measurements of 457 trees using both a laser hypsometer in the field and LiDAR systems (airborne or terrestrial), we confirm that the "sine" method results in a systematic bias of −7% in the *H*

estimations (Fig. 3). The way this bias propagates into AGB estimates through direct measurements or *H–D* models depends on whether a similar bias occurred in the destructive reference dataset used to build the AGB allometric model.

Beyond measurement errors, *H–D* allometric models represent a major source of uncertainty in field-based AGB estimates because this allometry exhibits large spatially structured variations at local, regional and continental scales (Ketterings et al. 2001; Feldpausch et al. 2011; Vieilledent et al. 2012; Vincent et al. 2012b; Réjou-Méchain et al. 2015). To account for broad-scale variations, both regionally averaged *H–D* relationships (Feldpausch et al. 2012) and bioclimatic proxies (Eq. 6 in Chave et al. 2014) have been proposed. These approaches significantly reduce AGB model errors in tropical regions, but certain local deviations may remain quite large. For instance, in the central Congo Basin, forest AGB was overestimated by 24% when the Feldpausch et al. (2012) regional *H–D* relationship was used instead of a local relationship (Kearsley et al. 2013). In the Khao Yai Forest Reserve in Thailand, we found that the bioclimatic proxy proposed by Chave et al. (2014) underestimated *H* by 26% (Jha, Chanthorn, Réjou-Méchain, unpublished). Finally, both approaches resulted in an AGB underestimation > 20% in a Brazilian forest (Hunter et al. 2013). Considering such uncertainty in only *H* estimations, any RS–AGB model calibrated in these regions would result in a systematic bias > ± 20% in AGB estimations (case B in Fig. 1), i.e. an error margin larger than the commonly admitted accuracy.

H–D relationships may also strongly vary between plots within landscapes. Average differences in *H* of approximately 10% for a given *D* were found between plots within areas < 10 km^2 in French Guiana (Vincent et al. 2012a, 2014; Réjou-Méchain et al. 2015). More specifically, the *H–D* relationship was found to strongly vary along a successional gradient in Thailand (Chanthorn et al. 2017); hence, this relationship varied concomitantly with forest AGB, potentially leading to a non-uniform bias in RS models (case of Fig. 1c). Various strategies may be adopted to better account for these inter-plot variations. The most straightforward strategy is to acquire *H* data for at least a subsample of trees to calibrate plot-specific *H–D* allometries (Vieilledent et al. 2012; Hunter et al. 2013), even though care must be taken with respect to the *H* measurement method and sampling strategy (see above and Sullivan et al. 2018). Another way to better account for systematic variations in *H–D* allometry between plots would consist of finding local covariates. Forest structural metrics that reflect stand competition intensity or soil fertility were found to explain some variation, but to a relatively small extent (Feldpausch et al. 2011; Banin et al. 2012). In contrast, mean canopy height has been found to correlate well with tree slenderness (a higher *H* for a given *D*), both within species and at the community level (Vincent et al. 2012a). Hence, when a high-resolution canopy height map is available, the accuracy of individual *H* estimations from *D* measurements can be significantly improved by adding local canopy height metrics to the *H–D* model (e.g., median of the canopy height model in a 50-m window centred on each tree). Using this approach, the individual *H* error was reduced by 14%, leading to a threefold decrease in the plot-level AGB bias at the Paracou site, French Guiana ($n = 2141$ trees; Vincent et al. unpublished). This result adequately illustrates that if field-based estimates generally feed into RS models, they may also themselves be improved by RS measurements. With the recent advances in our ability to extract individual trees from dense LiDAR point clouds (Ferraz et al. 2016), *H* measurements may be directly assigned to individual canopy trees that account for a large share of the stand AGB (Bastin et al. 2015b). In conclusion, better integration of LiDAR technologies and field measurements has the potential to substantially reduce the uncertainties associated with tree height variations.

2.3 Uncertainty in AGB Allometric Equations

The allometric conversion of individual tree attributes into AGB is a major source of uncertainty in tree and plot AGB estimates (Chave et al. 2004; Molto et al. 2013). At the tree level, the predictive error associated with the pantropical allometric model of Chave et al. (2014) reaches almost 40% (the total error is slightly above 50%), but if considered random, this error rapidly averages out as the number of trees increases in the predicted population (Réjou-Méchain et al. 2017). A cross-validation assessment of this model indeed revealed a mean bias across sites of only 5% but exceeded 30% in 8 out of 58 sites (Chave et al. 2014). Models that assume universal allometry may thus be liable to strong and uncontrolled local bias, which is generally ignored in error propagation schemes. This site effect may reflect differences in species composition or biotic (e.g., competition intensity) or abiotic (e.g., soil fertility) conditions. For instance, the use of biome-specific rather than species-specific allometries resulted in an AGB prediction bias between −18% and +14% for a Brazilian mangrove forest (de Souza Pereira et al. 2018).

Crown allometry variations among sites have also been identified as a major source of uncertainty in pantropical allometric models (Goodman et al. 2014). The proportion of the crown to the total tree AGB is indeed highly variable among trees (3–88%) and tends to increase with the increase in tree AGB beyond 10 Mg, reaching 50% on average for trees > 45 Mg and 34% for trees < 10 Mg (Ploton et al. 2016). This systematic change in tree shape with total tree AGB explained 20% of the underestimation of the AGB of large trees reported by Chave et al. (2014). Using simulations, Ploton et al. (2016) showed that, for 1-ha plots, this bias led to systematic errors ranging from −26% to +16% that depended on the frequency of large trees, thus introducing a non-uniform bias in AGB maps (Fig. 1c). Integrating crown dimensions in allometric models strongly reduces this allometric uncertainty. Jucker et al. (2017b) even proposed an AGB allometry using crown size and tree height, i.e. tree dimensions potentially directly measurable by means of RS (e.g., Ferraz et al. 2016).

Another potential source of uncertainty in the allometric conversion of tree attributes into AGB is the existence of hollow parts in the trunks or branches. Hollow parts are implicitly accounted for in AGB estimates when allometric equations are built on directly weighed trees. However, direct weighing is rarely possible for large trees, which are also more prone to hollows (Fig. 4). As a consequence, volume estimation is usually preferred for large trees (Henry et al. 2010; Fayolle et al. 2013; Chave et al. 2014), which results in potential estimation bias (Moundounga Mavouroulou et al. 2014). For instance, Nogueira et al. (2006) found that hollows occurred in ca. 10% of the trees > 5 cm in diameter in Brazil, but hollows occurred in up to 50% of trees > 80 cm in diameter (but $n = 4$ in that study). This condition, however, resulted in a bias ≤ 1% in the AGB in a 1-ha plot, which is consistent with the results of Clark and Clark (2000) in Costa Rica (hollow parts accounted for only 1.7% of the outer volume). Conversely, other studies reported much higher errors in other sites (Rodrigues and Valle 1964 cited in Nogueira et al. 2006; Dickinson and Tanner 1978), suggesting that the frequency of hollow trees may vary between sites and may also be a source of uncertainty in AGB maps. For instance, in over 523 forested sites in south-eastern Australia, the number of hollow trees strongly varied between sites with a skewed distribution, i.e. many study sites contained few or no hollow trees, but some sites contained up to 13 hollow trees per ha (Lindenmayer et al. 1991). Interestingly, the occurrence of hollow trees was well predicted by topography, stand age, region, logging history and the dominant species. Similarly, in a subtropical forest in China, the density of hollow

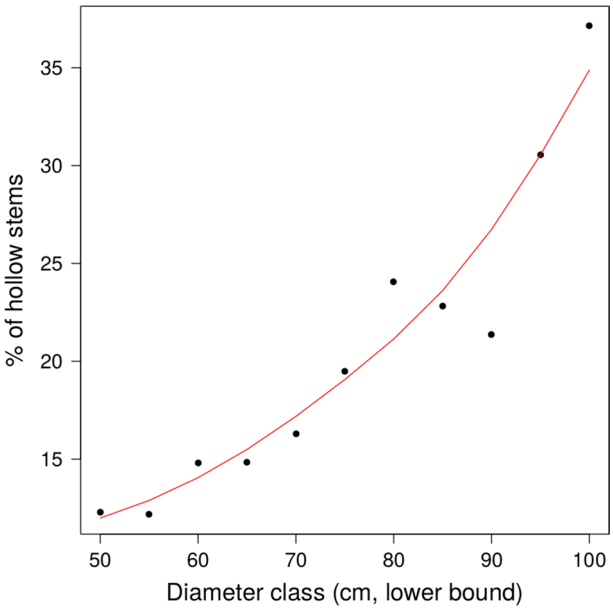

Fig. 4 Increase in hollow occurrence with tree diameter in a French Guiana dataset. In total, 17% of a sample of 3746 stems with DBH > 50 cm in French Guiana were found to be hollow. This proportion appeared to be strongly positively related to tree size. Courtesy of L. Descroix, unpublished

trees was approximately 90 trees per ha, which is much higher than that in temperate forests, and hollow occurrence varied significantly with species, crown position and topographical context (Liu et al. 2018). However, more studies are needed to better quantify the impact of hollows or simply wood decay on stand AGB estimates, using, for instance, non-destructive wood imaging techniques (Arciniegas et al. 2014). Marra et al. (2018) used sonic and electrical resistance tomography to identify internal wood decay without apparent cavities that resulted in C loss in the trunk ranging from 0.1 to 24% (5–37% with an apparent cavity).

2.4 Perspective on Field-Based AGB Estimation

The use of terrestrial laser scanners (TLS) has recently emerged as a credible alternative to destructive approaches for the estimation of tree AGB (Calders et al. 2014; Disney 2018; Gonzalez de Tanago et al. 2018; Lau et al. 2018; Momo Takoudjou et al. 2018). This technology and the associated processing methods are rapidly progressing but still face a number of challenges in tropical moist forests, such as the high degree of occlusion, the difficulty in segmenting individual trees in intricate vegetation (Trochta et al. 2017; Calders et al. 2018) and in filtering out leaves (Béland et al. 2014; Ma et al. 2016; Calders et al. 2018), which is a required step prior to tree structure reconstruction from the point cloud (Momo Takoudjou et al. 2018). Overcoming these issues would take us one step closer to an automated routine for reconstructing entire forest stands, thereby producing large amounts of data to feed allometric models (Raumonen et al. 2013). However, the above-mentioned problems associated with poor WD estimates and the presence of hollow trees remain a serious difficulty for TLS to overcome, which inherently measures the outer volume.

Another perspective from the advent of LiDAR technology is the possibility of directly estimating stand-level AGB instead of summing the AGBs of individual trees. For instance, Vincent et al. (2014) analytically derived a stand-level AGB equation based on stand volume-weighted WD, tree density, mean quadratic diameter and mean canopy height, which, as discussed above, controls the local *H–D* allometry. Stand density and mean quadratic diameter can both be extracted from TLS data (e.g., Bauwens et al. 2016) more accurately and more easily than individual tree volumes, while a canopy height model within a scanned plot can be derived from the same TLS data. Once such a relationship is calibrated, airborne laser scanners (ALS, including those on unmanned aerial vehicles (UAVs)) suffice to derive AGB estimates from standard stem diameter measurements and WD estimates. However, the calibration step is challenging because it would ideally rely on destructive stand-level measurements. Such an approach would probably limit the propagation of individual errors, especially when neither tree height measurements nor a reliable local *H–D* allometry is available.

3 Matching Field and RS Measurements

When an RS signal is related to a field-based estimate of forest AGB, the basic assumption is that they both measure the same area and objects. This assumption is often violated in practice, leading to large uncertainty in the final AGB density maps (Gobakken and Naesset 2009; Frazer et al. 2011; Mascaro et al. 2011; Réjou-Méchain et al. 2014; Saatchi et al. 2015). Here, we review important sources of mismatch between field and RS measurements and identify ways to overcome them.

3.1 Geolocation Uncertainty

Geolocation mismatch between RS and field measurements is an obvious source of uncertainty (Frazer et al. 2011). Ground measurements are generally geolocated using a global navigation satellite system (GNSS) receiver, whose accuracy is known to vary with receiver quality or topographical and vegetation conditions by up to 2 orders of magnitude (Johnson and Barton 2004). In particular, GNSS accuracy decreases exponentially with the increase in canopy cover (Sigrist et al. 1999). From simultaneous acquisitions, Johnson and Barton (2004) found that 20% of the measurements had geolocation errors > 10 m under forest cover (due to multipathing effects), but only 2% in a nearby open area. Under unfavourable satellite conditions, the error even exceeded 200 m under forest cover. Under a dense forest cover in Gabon, a recent high-grade GNSS resulted in a mean measurement error of 5 m with 2.5% of extremes greater than 70 m (Fig. 5; Réjou-Méchain and Barbier, unpublished). Differential GNSS corrections did not reduce this uncertainty because vegetation cover prevents the use of phase-shift information. However, geolocation errors rapidly averaged out as the number of measurement points increased in either space (over a few tens of metres) or time (over several hours or days), stabilizing below 5 m with 20 measurement points and below 3 m with 50 measurement points. This result confirms the recommendation of Segrist et al. (1999) to collect at least 20 GNSS measurement points at different locations or times to accurately geolocate a field plot in dense forest conditions.

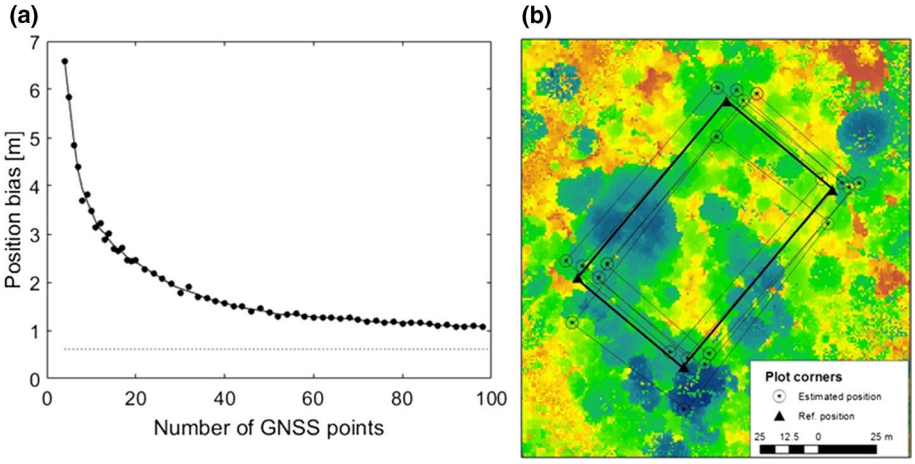

Fig. 5 Plot positioning error in a dense forest from Gabon. **a** The 75th percentile of mean position bias as a function of the number of GNSS points taken along plot limits from random point sets taken among 207 GNSS points (using a Trimble L1/L2 GEOXT 7000 rover GNSS device). The dotted line represents the background error level (e.g., due to imperfections in the relative positions of field marks). **b** An example of plot position bias for a 60×100 m plot at the 75th percentile of the error distribution using random sets of 4 GNSS points to estimate the transformation from local to UTM coordinates. Reference positions were provided by a professional topography consultant using a total station. Background colours show maximum canopy height (from brown to blue) from terrestrial laser scanning data

3.2 Acquisition Angle

Satellite-borne instruments do not always measure forests vertically (i.e. in nadir mode). When an active penetrating signal (e.g., RADAR or LiDAR) is sent with a large (pluri-metric) footprint size and a significant incidence angle (typically $> 30°$ for RADAR sensors; Saatchi et al. 2011a; Robinson et al. 2013), the forest volume measured in field plots and intercepted by the satellite sensor does not correspond to the same physical objects, especially for small plots or in topographically complex areas (Villard and Le Toan 2015). Using theoretical simulations, Réjou-Méchain and Barbier (unpublished) found that an incidence angle of 30° may lead to volume differences of ca. 55, 20 and 10% for plot and pixel sizes of 20, 50 and 100 m, respectively, even if existing surrounding trees partly compensate for this mismatch. Thus, any RS signal acquired with a significant incidence angle should not be calibrated and validated with small field plots or in small patches of heterogeneous vegetation.

3.3 Mismatch in Tree Representation

The mismatch between the RS and field measurements may also be due to differences in tree representation. Conventional field measurements for AGB estimations are "trunk-based", i.e. a tree is considered to belong to a given field plot when half its trunk base section is within the plot limits, irrespective of the proportion of its vertical crown projection falling outside the plot. With RS approaches, AGB is measured from an area-based perspective, i.e. only the plant material with a ground projection within the area of interest is considered. Using LiDAR data, Mascaro et al. (2011) showed that

accounting for this edge effect reduces the LiDAR-AGB model error by 55, 21 and 4% at 20-, 50- and 100-m resolution, respectively, i.e. with a decrease in the perimeter-to-area ratio, the associated edge effects logically vanish because the proportion of trees with crowns crossing the plot edge decreases with the increase in plot size.

Differences in tree representation may also impact the estimates of forest C dynamics. Réjou-Méchain et al. (2015) compared the 4-year AGB dynamics inferred from repeated field plot censuses and LiDAR acquisitions and found relatively poor agreement between the two estimates; these authors concluded that different components of forest dynamics are measured by the two approaches. Natural canopy dynamics is dominated by many small-scale events that are captured by LiDAR data but not by field measurements (Kellner and Asner 2009; Leitold et al. 2018). Similarly, leaf density, which influences LiDAR estimates but not field estimates, regenerates faster than woody biomass after a disturbance (Asner et al. 2006). Thus, any dynamics inferred from RS measurements should be interpreted differently from the dynamics inferred from the ground.

3.4 Temporal Mismatch

The temporal difference between RS and field measurements is a common problem in RS studies. The impact of such temporal mismatches is difficult to predict in natural forests due to the high stochasticity of tree mortality. This stochasticity, however, decreases with the increase in plot size (Chambers et al. 2013); hence, the error associated with the temporal difference between measurements is likely to decrease with increasing plot size in the absence of major climate anomalies (e.g., El Niño events) or major disturbances, such as hurricanes or fires, which may be detected with Landsat (Kennedy et al. 2010) or MODIS (Justice et al. 2002) time series data. (MODIS is the Moderate Resolution Imaging Spectroradiometer aboard the NASA Terra and Aqua satellites.) In this case, estimated growth rates may be used to compensate for the time lag in AGB estimates from field and RS data (Avitabile and Camia 2018).

3.5 Scale Mismatch

The issue of scale mismatch between calibration field plots and RS data pixels is challenging, particularly when coarse-resolution RS products are calibrated with numerous small field plots such as national forest inventory data collected in sampling units less than 0.1 ha in size. For instance, the pantropical 1-ha resolution AGB map of Saatchi et al. (2011b) was calibrated using field plots that were typically ≤ 1 ha in size, hence representing a local sampling rate of 1% at best. For instance, Réjou-Méchain et al. (2014) showed that the use of calibration plots smaller than the RS pixels generates large sampling errors, producing significantly biased AGB maps (case Fig. 1c). For a given pixel-to-plot size ratio, the error due to local AGB variability is larger for small plots and pixels than for large plots and pixels (Réjou-Méchain et al. 2014). Thus, studies aiming at building coarse-resolution maps face the challenge of minimizing this sampling error. A common practice is to spatially aggregate field estimates to better match the RS pixel resolution; however, this approach results in large uncertainty in the associated sampling error (Avitabile and Camia 2018). A more reliable approach consists of using intermediate-resolution RS data, such as very high-resolution images, to bridge the gap.

4 Bridging Field and Satellite-Based Measurements

Field plots are generally too costly and time-consuming to establish to be densely and evenly distributed within landscapes. Consequently, RS models are often calibrated with field plots that are not representative of the area of interest (Marvin et al. 2014). Furthermore, field plot size rarely approaches the size of coarse-resolution RS pixels (e.g., MODIS, ca. 250 m), which are the current basis of the wall-to-wall biome or global mapping. This problem generates the mismatch issues discussed in the previous section. To overcome these problems, a multi-step upscaling approach involving RS data of very high spatial resolution (VHSR) can provide intermediate-scale biophysical maps to be then used as reference to calibrate wall-to-wall RS data of coarse resolution and broad swaths (Asner et al. 2013; Baccini and Asner 2013; Xu et al. 2017). In this section, we first review the VHSR RS products that may be used in such an approach and then discuss the caveats and perspectives associated with such a multi-step upscaling strategy.

4.1 Airborne LiDAR

Airborne LiDAR (ALS), with its ability to penetrate the canopy, provides a fine 3D description of the forest structure and represents an excellent option for linking field plots to broad-scale RS data. Over the last decade, a large number of studies have aimed at retrieving forest AGB from LiDAR-derived metrics, usually with good accuracy at the 1-ha scale (i.e. with a model prediction error typically below 15%; Zolkos et al. 2013). ALS allows for the computation of a variety of metrics related to the vertical or horizontal forest profile (Lefsky et al. 2002). Many studies have relied on statistical fittings (e.g., stepwise linear models) to identify the most predictive metrics in a given context, resulting in site-specific ALS–AGB model forms with limited transferability across sites (Vincent et al. 2012b; Zolkos et al. 2013). For this reason, some studies aimed at designing generic ALS–AGB models that were expected to perform consistently across sites. For instance, Bouvier et al. (2015) identified predefined metrics of strong complementarity and interpretability to build a generic model transferable across temperate forest types. In the tropics, another attempt used a single ALS metric, the mean top-of-canopy height (TCH), combined with minimal field data to predict forest AGB. Asner and Mascaro (2014) used data from 14 tropical areas to calibrate a model of the form $AGB = a TCH^{b1} BA^{b2} WD^{b3}$, where the basal area (BA) was locally predicted from TCH, and where WD relied on regional estimates. However, the fitted equation, which was presented as universal, led to underestimations of 7% (Jucker et al. 2017a) and 16% (Réjou-Méchain et al. 2015) in two independent sites compared with locally adjusted models. A modification of the model form was suggested by Vincent et al. (2014), where the scaling of AGB estimates from tree to plot used the stem number (N) and average stem cross-sectional area (or quadratic diameter) instead of BA to avoid unwarranted errors in the scaling process. A universal predictive equation that relates ALS metrics and AGB should continue to be sought to maximize the benefits from the increasing availability of ALS data (Labriere et al. 2018). However, as long as *H–D* variability is not accounted for, a single predictive equation would remain elusive. Furthermore, airborne data acquisition remains costly (ca. 200–500€ km^{-2}) and is subjected to flight authorization, which hampers ALS acquisitions in certain countries.

4.2 Unmanned Aerial Vehicle (UAV) Systems

UAVs may reduce the cost of airborne acquisitions and are thus increasingly utilized. UAV systems can generate 3D point clouds through the acquisition of very high-resolution passive imagery. The overlap between UAV acquisitions enables stereoscopic image processing with potentially very high spatial resolution and low cost compared to LiDAR systems (Puliti et al. 2015). Under the generic appellation of structure-from-motion approaches, the automation of traditional photogrammetry by the detection of invariant features in 2D images allows for the derivation of dense point clouds (Fig. 6). However, such systems mostly capture variation in the top of the canopy and have a rather low ability to penetrate dense forests, limiting the computation of forest height metrics (Roşca et al. 2018). UAV-borne LiDAR systems are rapidly developing but are still relatively new (Brede et al. 2017). With an optimized sampling strategy, these systems are able to generate a large number of points (thousands of pts m^{-2}), opening the door for individual tree volume reconstruction using toolboxes developed for TLS (Morsdorf et al. 2017), even if UAV-specific methods would be preferable due to an inverted vertical distribution of point density. However, flight authorization remains an issue in some countries, and even where authorized, maximum legal UAV piloting distances limit the acquisitions to rather small areas (e.g., ca. 300 ha in France).

4.3 VHSR Spaceborne Systems

Spaceborne data may be mobilized to complement ALS or UAV data and move beyond the relatively small extents of ALS and UAV campaigns, notably because these data can be acquired at a low cost and with few issues regarding authorizations. For instance, VHSR satellite optical images ($\leq$2 m resolution) are able to characterize canopy texture, which informs the size distribution of canopy crowns and inter-crown gaps (Couteron et al. 2005; Frazer et al. 2005), thus indirectly informing stand structure and AGB. Texture has historically been widely used in forest science for visual interpretation of aerial photographs. Similar interpretations from automated processing can be carried out from VHSR images via canopy texture analysis whenever images have sufficient effective resolution (the maximum acceptable seems to be approximately 2 m; Proisy et al. 2007). For instance, the Fourier-based textural ordination (FOTO) method aims to ordinate canopy image windows along texture gradients based on Fourier spectra (Couteron et al. 2005), and this method successfully retrieved the AGB gradients in several case studies across the tropics with an accuracy only slightly lower than that of ALS approaches (relative prediction error $\leq$20%; Proisy et al. 2007; Ploton et al. 2012; Bastin et al. 2014; Singh et al. 2014; Pargal et al. 2017) but at 50–100 times lower cost (2–10€ km^{-2} for optical images). Hence, the trade-off between data interpretability versus affordability should suggest designing scaling-up strategies based on nested sampling of field, airborne and VHSR satellite data. Satellite-borne optical sensors offering VHSR may thus be part of an effective chain for mapping AGB at landscape-regional scales. However, there are also situations in which texture analyses fail to properly retrieve certain AGB gradients (Ploton et al. 2013; Blanchard et al. 2015) because the way in which texture features relate to AGB strongly varies across forest types (Ploton et al. 2017). Due to the limited number of field plots available for calibration and validation, biophysical drivers of canopy texture have not been fully identified in previous studies. The increasing availability of ALS data will help to better evaluate such texture-based approaches and ultimately allow for the calibration and validation of texture indices in sufficiently diverse forest types. However, canopy texture,

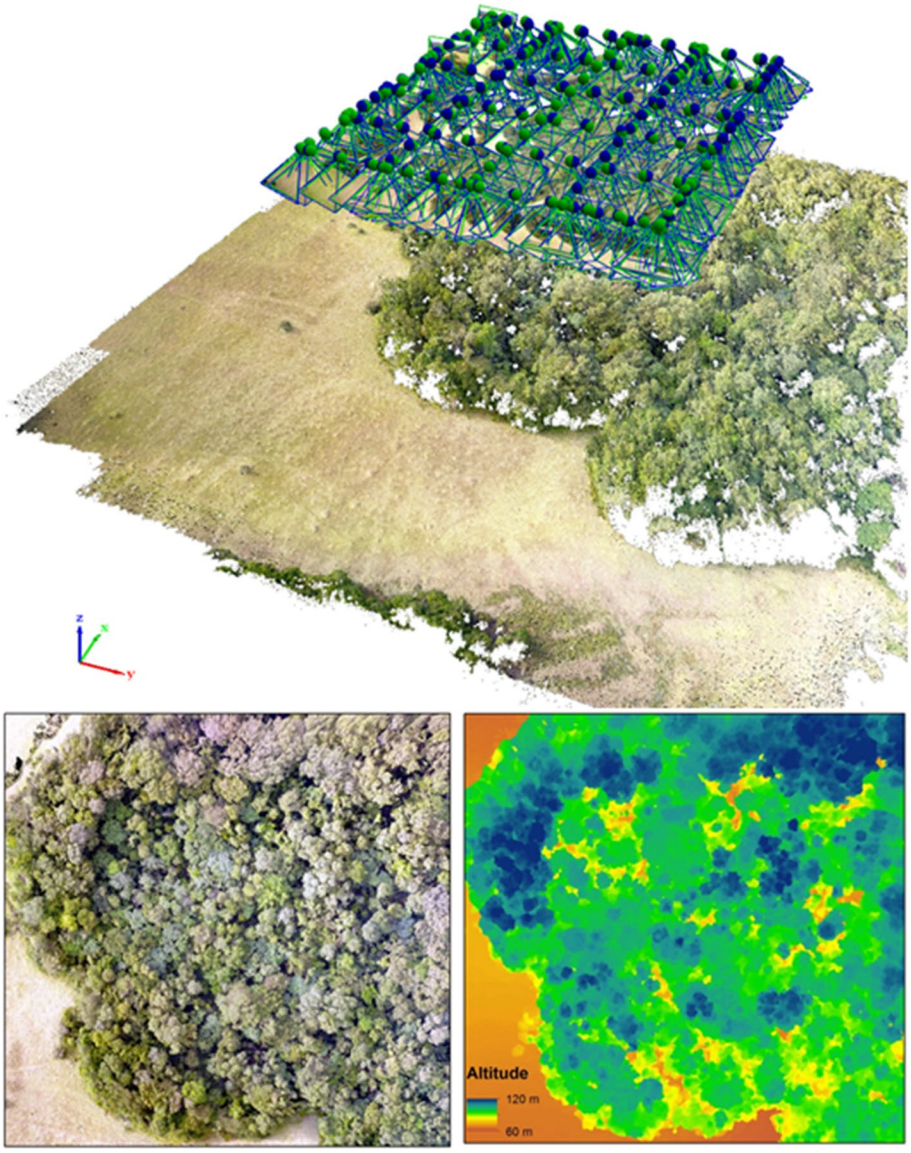

Fig. 6 Illustration of the structure-from-motion approach allowing for the derivation of an orthomosaic (lower left) and a surface model (lower right) by automated stereophotogrammetry from drone imagery (upper panel) in a forest-savanna mosaic from central Cameroon

such as reflectance, is strongly impacted by the Sun–scene–sensor geometry, although correction techniques have been proposed (Barbier et al. 2011; Barbier and Couteron 2015). The number of textural descriptors, therefore, needs to be kept to a minimum to control these effects in large collections of images acquired in diverse geometrical configurations.

Apart from texture indices, stereophotogrammetric approaches from VHSR satellite images allow for the retrieval of canopy surface models that may then be used to predict

AGB. This retrieval implies more cloud-free images and a higher budget for data acquisition and, contrary to LiDAR, stereophotogrammetric approaches do not provide information on fine-scale topographical variation, which is detrimental for building canopy height models. Thus, such approaches remain very scarce in the literature (St-Onge et al. 2008; Lagomasino et al. 2015). Finally, non-penetrating X-band RADAR satellite images used in stereo mode (Tandem-X) have also shown to have the potential to predict AGB gradients linked to logging and forest degradation and to assess AGB losses through diachronic comparisons (Schlund et al. 2015; Solberg et al. 2018).

4.4 Limits and Perspectives on Bridging Field and Satellites

Regardless of the VHSR product or model structure used for bridging field plots and large-scale RS data, there are several caveats. First, both the number of calibration field plots and their size remain important for restricting VHSR-based AGB prediction errors to acceptable limits. For instance, in a meta-analysis of LiDAR-based AGB estimations, Zolkos et al. (2013) showed an asymptotic decrease in the prediction error with the increase in the size of the calibration plots, with a slow decay on average above a plot size of 0.2 ha, corresponding to a prediction error of ca. 20%. However, highly contrasted results can be found across case studies, suggesting that prediction errors vary with forest structure at a given plot size. For instance, in tropical forests of Ghana, Chen et al. (2015) found a LiDAR-based prediction error on AGB of ca. 42% at a spatial resolution of 0.16 ha. Thus, AGB estimates derived from VHSR data and used for calibrating broad-scale products should be performed at a rather coarse resolution, with 1 ha being a conservative resolution to ensure an acceptable accuracy.

Another major problem that may arise during the plot to VHSR step is that significant biases may occur during the extrapolation of plot AGB estimates through the VHSR products. For instance, the prediction of AGB from local stand height or related RS metrics relies on knowledge of local WD and height–diameter allometry. As discussed in Sect. 2, both measures are known to vary, sometimes abruptly, within landscapes, and there is thus no guarantee against biases when extrapolating AGB estimates over areas where these variations are unknown. Stratifying the landscape by forest types prior to AGB model calibration thus appears essential to guarantee model robustness, although there are not many accounts of thorough pre-stratification processes in the literature (Gregoire et al. 2016). However, sources of complementary data are developing. Notably, hyperspectral sensors now appear to able be to provide information on canopy species composition and help infer WD (Jucker et al. 2018b). Moreover, some LiDAR metrics (e.g., canopy gap fractions) can help assess the disturbance or successional status of the forest with relevance for the explicit estimation of WD (Guitet et al. 2018).

5 Global Wall-to-Wall Extrapolation

Earth system models and international policy initiatives both require wall-to-wall data (Sitch et al. 2008; Romijn et al. 2018; Herold et al. 2019). Thus, there is a strong need for going beyond local to regional AGB estimates to produce unified AGB density maps at the biome or global scale. Pantropical, temperate, boreal and global AGB maps have been proposed in the last decade, most often by extrapolating field-based and/or LiDAR-based AGB

estimations through the use of global optical, RADAR and environmental datasets. In this section, we discuss the issues associated with large-scale AGB mapping and the promise of new methods and upcoming spaceborne missions.

5.1 The Problem of Interpolation

None of the RS systems available to date that display fair to good correlation with AGB (with no signal saturation) offers wall-to-wall coverage at very broad scales (i.e. regions, countries, continents). At best, these systems provide a fairly systematic sampling of the earth surface under the form of belt transects (e.g., ICESat/GLAS or the upcoming GEDI and MOLI missions). This condition implies that an interpolation step is necessary to produce a continuous AGB map from this discrete sampling. To that end, all published approaches have used or combined statistical interpolation (e.g., kriging or co-kriging with environmental drivers) and predictions from high- to medium-resolution spaceborne RS data to produce wall-to-wall coverage (e.g., Landsat, MODIS, QuickScat, ALOS PALSAR). For instance, Saatchi et al. (2011b) and Baccini et al. (2012) mapped AGB over the tropics by spatially interpolating discrete AGB estimates using Quick Scatterometer and/or MODIS data. Avitabile et al. (2016) then combined these two maps and used additional reference data (field plots and locally calibrated maps) in an attempt to generate an improved AGB map. Finally, the map from Santoro et al. (2018) was derived at 100-m resolution using a combination of maps based on ALOS PALSAR, ASAR data, Landsat data and ICESat GLAS transects, without any calibration from in situ data.

The use of these RS data for estimating AGB at a large scale raises two problems, which remain largely unsolved. First, most current satellite-based data relate to signals for which relationships to AGB are saturating and/or highly context-dependent (Steininger 2000), due to either varying relationships between AGB and RS signals or signal artefacts. Optical images are affected by geometrical and atmospheric effects that may produce significant spatial and/or seasonal artefacts in surface reflectance (Morton et al. 2014). For instance, the high degree of cloudiness in western Gabon and Cameroon is known to strongly impact MODIS reflectance data and is likely the reason why Baccini et al. (2012) underestimated the AGB values in this region (Fig. 7). Similarly, RADAR data are affected by factors related to forest structure and the environment (e.g., soil and vegetation moisture, topography) and the uncertainties associated with RADAR data acquisition (Villard and Le Toan 2015). Second, in natural tropical forests, stand structure variables often strongly vary over short distances. Variograms computed on field plot networks reported spatial correlation in AGB or BA that barely reached 5 km (Guitet et al. 2015; Hajj et al. 2017). This result means that locations that are more than 4–5 km apart are virtually independent; thus, any reliable AGB estimate conveys no useful information for interpolation beyond this distance.

Thus, it is not surprising that strong inconsistencies have been reported among broad-scale AGB maps (Mitchard et al. 2013; Huang et al. 2015; Rodriguez-Veiga et al. 2017). For example, Mitchard et al. (2013) compared two widely used pantropical maps (Saatchi et al. 2011b, Baccini et al. 2012) and found fairly consistent estimates at the continental scale but large regional differences (> 100%) within continents. In Amazonia, a comparison with field estimates suggested that both pantropical maps failed to capture the AGB gradient across regions with some regions over- or underestimated by > 25% (Mitchard et al. 2014). However, without a systematic field sampling of AGB at a large scale, as done

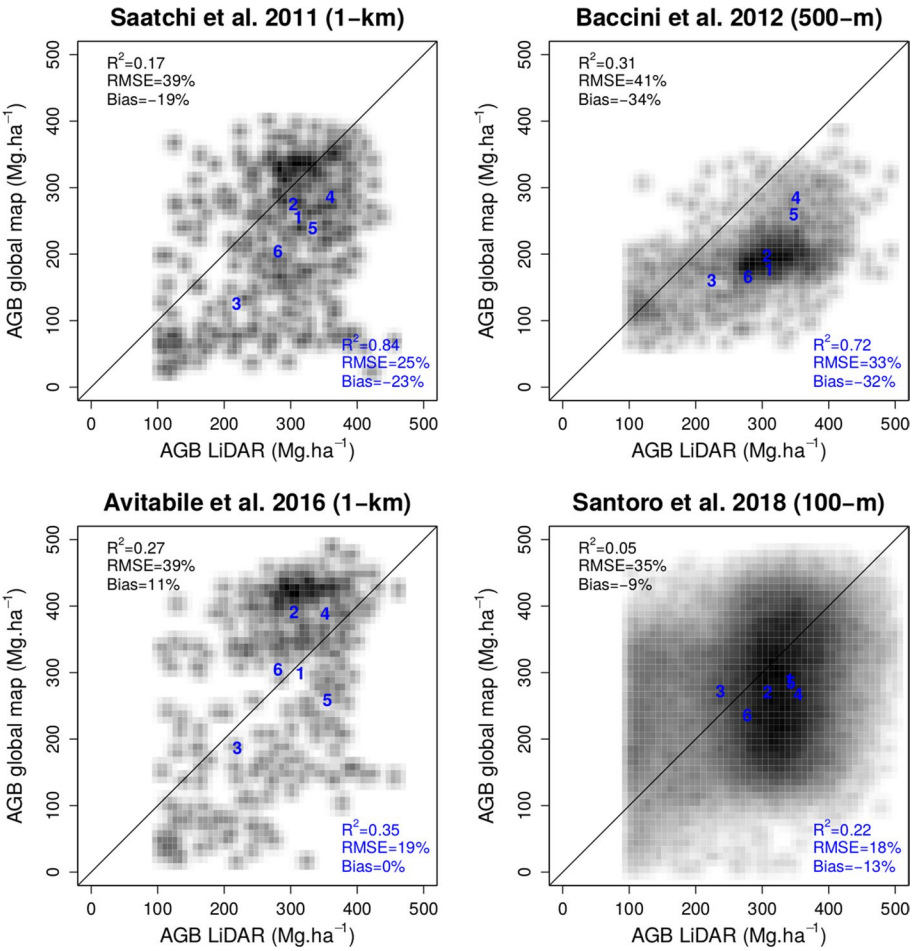

Fig. 7 Validation of global and pantropical maps using independent AGB estimates from six airborne LiDAR (ALS) campaigns in French Guiana and Gabon in forests > 100 Mg ha^{-1}. The results are reported at both the pixel (black) and mean AGB site (blue) level (1: Lope; 2: Mabounie; 3: Mondah; 4: Nouragues; 5: Paracou; 6: Rabi). ALS–AGB density maps at 50 m resolution were first resampled to the resolution of the pantropical and global maps using the Geospatial Data Abstraction Library (GDAL) *gdalwarp* routine in average mode. ALS- and global AGB density maps were then superimposed using bicubic interpolation (Inglada and Vadon 2005) through the *otbcli_Superimpose* routine of the Orfeo ToolBox (https://www.orfeo-toolbox.org/). Spatial correlations using fast Fourier transforms in moving windows confirmed that the spatial match between both AGB estimates was high (uncertainty was below the pixel resolution)

in national forest inventories (Kleinn 2017), it is difficult to validate whether a map captures the regional AGB gradients.

In Fig. 7, we report the result of a comparison of five existing pantropical/global AGB maps with six LiDAR-based AGB maps from Africa and French Guiana (Labriere et al. 2018). The results confirm that in dense forests (> 100 Mg ha^{-1}), broad-scale maps display relatively weak ($R^2 \leq 0.3$) if any correlation at the pixel level with independent AGB data of improved quality. However, some maps exhibit much higher correlations than others considering the very coarse-resolution gradients (here the mean AGB per LiDAR site),

with the R^2 value for the map of Saatchi et al. (2011b) exceeding 0.8. Although this result is based on six observations and should be confirmed with more sites, it could suggest that broad-scale AGB variations may be successfully captured with such maps. These comparisons shed some light on the uncertainty associated with these AGB map estimates, but they also convey their own errors for validation or accuracy assessments for at least two reasons. First, the maps are all produced for different time periods, e.g., the Saatchi et al. (2011b) map is for ca. 2000, the Baccini et al. (2012) map is for ca. 2008 and Avitabile et al. (2016) combined these two maps using ground- and LiDAR-estimated AGB at different spatial scales and time periods. Second, the definition of forest and AGB may be different for each map. In Saatchi et al. (2011b), the biomass estimate at 1 km referred to the biomass of remaining forest in each 1 km grid cell, whereas in all other maps, the estimates referred to the mean biomass at the grid cell of the map (average of forest and non-forest biomass).

5.2 The Use of Environmental Proxies

One possible way to mitigate the aforementioned difficulties that hinder interpolation is to rely on spatialized environmental proxies to enhance the mapping. In the central Amazon, Saatchi et al. (2007) used a multivariate decision tree approach featuring both environmental variables (e.g., elevation, climate) and saturating RS metrics (e.g., Qscat_SV, NDVI) and found that AGB classes referring to values above 250 Mg ha^{-1} were mainly located in areas below 190 m elevation and of limited ruggedness (both assessed from SRTM). AGB is indeed known to covary with topography globally (Réjou-Méchain et al. 2014), but the strength and direction of the relationship strongly vary across sites (de Castilho et al. 2006; McEwan et al. 2011; Detto et al. 2013; Réjou-Méchain et al. 2015). Some studies successfully relied on spatialized climatic variables (Simard et al. 2011; Fayad et al. 2016) or geomorphological units (Guitet et al. 2015) to predict AGB or forest height in particular regional contexts. Thus, the ongoing development and improvement of global databases of environmental variables open avenues for geographically enlarging such approaches bearing in mind that relationships between AGB and the environment are intrinsically context-dependent. Indeed, AGB is largely driven by complex edaphic processes, such as soil structure (Gourlet-Fleury et al. 2011; Jucker et al. 2018b) or water table and bedrock depth (Emilio et al. 2013), which often vary at a relatively fine scale and for which continuous information is lacking. Furthermore, past and present anthropogenic activities, which are not randomly distributed according to abiotic conditions, may largely blur such environmental determinism at large scales. Therefore, calibration and prediction should be designed according to a relevant pre-stratification of the territory, accounting for anthropogenic activities, with sufficient reference data in each stratum.

5.3 Perspectives on Extrapolation

Upcoming RADAR satellite missions, such as NISAR in 2021 (Rosen et al. 2017) and BIOMASS in 2022 (Le Toan et al. 2011), should be pivotal in global-scale AGB mapping by providing wall-to-wall active measurements. While NISAR will be relevant for low AGB areas due to the use of an L-band saturating signal, BIOMASS will operate with a 50-m resolution P-band signal that is sensitive to large AGB values. (AGB products will, however, be delivered at 200-m resolution.) Preliminary analyses from P-band airborne missions revealed that polarimetric intensities (PolSAR) and polarimetric RADAR

interferometry (PolInSAR) correlated well with AGB values up to 300 Mg ha^{-1} in temperate and tropical areas (ESA 2012). Above 300 Mg ha^{-1}, such approaches failed to detect AGB variations, but tomographic approaches may significantly improve the retrieval of AGB up to 500 Mg ha^{-1} with no obvious saturation and a prediction error of only ca. 10% at a 1.5-ha resolution (Minh et al. 2014). A cross-validation performed between two sites of tropical forests in French Guiana suggested that tomographic models are transferable with an error within 20% at 1-ha resolution (Minh et al. 2016). However, these approaches rely on multiple acquisitions with different geometries over the same site, constituting a challenge for a spaceborne sensor and limiting the areas that may be covered in such a way. As a consequence, tomography will be implemented in only the first year of the mission; the three subsequent years will instead correspond to an interferometry phase. Beyond AGB mapping, the upcoming missions, including GEDI and MOLI, also constitute a unique opportunity to better understand the relationship between forest AGB, productivity and spatialized environmental proxies in tropical dense forests.

Finally, if future missions will considerably improve our ability to monitor AGB in space and time, the full potential of current RS products has not yet been completely assessed. For instance, using multi-angle MODIS observations to characterize the anisotropy of forests, de Moura et al. (2016) were able to generate metrics that displayed a good correlation ($r^2 > 0.5$) with ALS-derived metrics in high AGB forests in the Brazilian Amazon, with no apparent saturation. This result adequately illustrates that there is also room for progress through the development of new methodologies to be used with the current RS products.

6 Radiative Transfer Modelling for Understanding Error Sources

A prerequisite to controlling the sources of errors in satellite-based assessments of forest AGB is to understand how the electromagnetic signal of interest interacts with forest components. Contrary to sea surface temperature, for instance, there is not yet any sensor that directly measures woody AGB per se. We thus use the variations in proximal measurements or indices to infer the AGB variations; however, these measures may be prone to interferences and artefacts that sometimes blur the true response of the forest AGB. Thus, radiative transfer (RT) modelling has become a standard approach in RS to analyse sensor sensitivity, and inverse modelling is used to measure the extent at which specific forest information is recoverable from the recorded signals. Some recent prominent examples can be found in studies that investigated the seasonal variation in leaf area in tropical forests (Morton et al. 2014; Wu et al. 2018) or texture retrieval of forest AGB from VHSR optical images (Ploton et al. 2017). Even crude modelling approaches may prove useful to untangle complex interactions in the sensor–atmosphere–scene–light source system (Barbier et al. 2011; Barbier and Couteron 2015), but a key point in such simulation studies is the way in which the complex 3D organization of tropical forest components can be represented. We will focus here on examples involving passive and active optical signals, but similar progress can be observed in RADAR studies (Villard 2009), which were historically pioneering (Ishimaru 1978).

6.1 An Increase in Model Realism

In the early days, geometric-optic models were used to understand the variation in directional reflectance within large pixels comprising a number of objects (e.g., trees) (Egbert 1977; Li and Strahler 1992; Roujean et al. 1992; Ni et al. 1999). Scene reflectance was computed as the sum of nominal reflectance of the components (e.g., shaded and lit surfaces) of a projection of simple, generally opaque, geometrical shapes within a scene. These efforts allowed for the derivation of analytical functions (kernels) that proved useful to fit actual directional reflectance variations with a small number of parameters (e.g., Lyapustin et al. 2011).

As computing power increased, it became possible to increase scene complexity, as well as to improve the level of detail in the descriptions of light–matter interactions. Discrete ray-tracing models based on Monte Carlo simulations of photon behaviour and (multiple) scattering within the scene have now become standard. This phenomenon is, for instance, evidenced by the periodic RAMI (RAdiation transfer Model Intercomparison) experiment, which aims at benchmarking and testing a number of existing models (Widlowski et al. 2013). Initially, scenes represented homogeneous parallel layers (Verhoef 1985; Myneni et al. 1989) of a turbid medium, in which the macroscopic transfer equation was statistically deduced from the microscopic distribution of elements, such as leaves or aerosols, within the cell. These elements were characterized by a density and angle distribution, as well as optical properties, which imply a probability of intercepting light rays depending on the incoming and outgoing directions. In addition to turbid elements, solid surfaces can be added in the form of triangle meshes to represent scene elements other than leaves (woody parts, roads, ground, building or water bodies). Triangles can be translucid and display Lambertian, specular or other optical properties. Progressively, spatial heterogeneity was introduced in the turbid medium distribution (Myneni 1991; Gastellu-Etchegorry et al. 1996; North 1996). Indeed, as opposed to most annual crops, crown shading is fundamental to understanding scene reflectance in forests. This fundamental need is even more pronounced when the spatial resolution of a sensor increases to a point where the pixels are smaller than the tree crowns, as biophysical descriptors can then be found in the texture features, and describing the spatial arrangement of reflectance values is crucial (Couteron et al. 2005; Barbier et al. 2011; Barbier and Couteron 2015). The degree of realism of a 3D description has evolved from sets of floating spheres or ellipsoids to more complex envelopes describing tree crown contours (Cescatti 1997; Widlowski et al. 2013). The dimensions and spatial distributions of these envelopes can generally be inferred from standard forestry measurements or allometric equations (Barbier et al. 2011).

To further improve the realism of the forest scenes, LiDAR data constitute a giant leap forward, as they provide both access to a detailed description of the geometry and topology of solid surfaces (trunks and branches) and a statistical sampling of foliage directly compatible with the turbid representation via voxelization procedures accounting for spatial sampling variations (Grau et al. 2017; Tymen et al. 2017; Vincent et al. 2017). In a temperate montane forest, a voxel-based approach performed better at simulating hyperspectral data than an approximation of individual tree envelopes (Schneider et al. 2014). Given the importance of LiDAR technology in detailed measurements of vegetation from space, air or ground stations, simulating the transfer of this active signal in vegetation is now itself an active field of study (Sun and Ranson 2000; Gastellu-Etchegorry et al. 2015). Figure 8 illustrates the current possibilities and challenges for the realistic simulation of dense tropical forests. On the one hand, the integration of the structure derived from airborne LiDAR

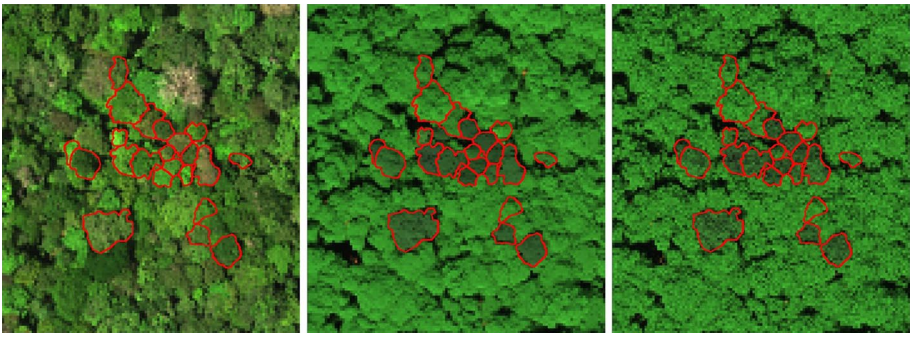

Fig. 8 Simulation of airborne optical imaging in a tropical forest from French Guiana (Paracou). The simulation is based on the integration of airborne LiDAR and field spectroscopy in the DART 3D radiative transfer model (Gastellu-Etchegorry et al. 2015). The 3D mock-ups were computed from airborne LiDAR point clouds using AMAPvox (Vincent et al. 2017), and leaf optical properties corresponding to sampled trees (delineated in red) were measured with a field spectroradiometer and assigned to leaf elements from all voxels on the vertical column of the mock-up. A generic set of leaf optical properties was applied to all trees with undocumented leaf optical properties using the PROSPECT leaf model (Féret et al. 2017). Left: original image (red = 640 nm; green = 549 nm; blue = 458 nm); centre: simulation using a turbid representation for leaf elements; right: simulation using triangle approach for leaf elements

acquisitions allows accurate simulation of canopy grain and gaps with metric resolution. On the other hand, the lack of information about the proportion of leaf versus woody elements (Malenovskỳ et al. 2008) and the difficulty in accurately characterizing the diversity of leaf optical properties at the canopy scale contribute to the relatively low radiometric agreement. Better accounting for the differences in radiometric properties among species or individuals and possibly within individuals would require a better understanding of the spatial heterogeneity of spectral properties (Féret and Asner 2014; Rocchini et al. 2018).

6.2 Limits and Perspectives on RT Modelling

The current difficulties that need to be overcome to effectively derive forest mock-ups from TLS data are the same as those mentioned above for deriving AGB estimates from TLS. For instance, individual tree segmentation is required to allocate species-specific radiometric properties to individual trees. In addition, accurate segmentation of leaves from wood and proper estimation of leaf angle distribution are required to accurately simulate light–vegetation interactions (Antin et al. 2015). These steps become more difficult in the upper canopy as the density of the TLS point cloud decreases dramatically due to occlusion and increasing distance from the laser source. This difficulty may, however, be minimized through the fusion of TLS and UAV data. Finally, a better understanding of leaf demography and its integration into advanced modelling of leaf optical properties, combined with the improved description of non-photosynthetic tissues in LiDAR-derived 3D mockups, will increase the realism of simulations derived from physical modelling.

An alternative to producing a forest scene with a turbid description of leaves is to use an architectural model to simulate the tree branching structure and individual leaf distribution (De Reffye et al. 1995; Dauzat et al. 2001; Côté et al. 2011; Widlowski et al. 2013; Calders et al. 2018). Independently of the biological realism of such detailed scene descriptions, these models provide a means to assess the degradation of the transfer modelling outcome

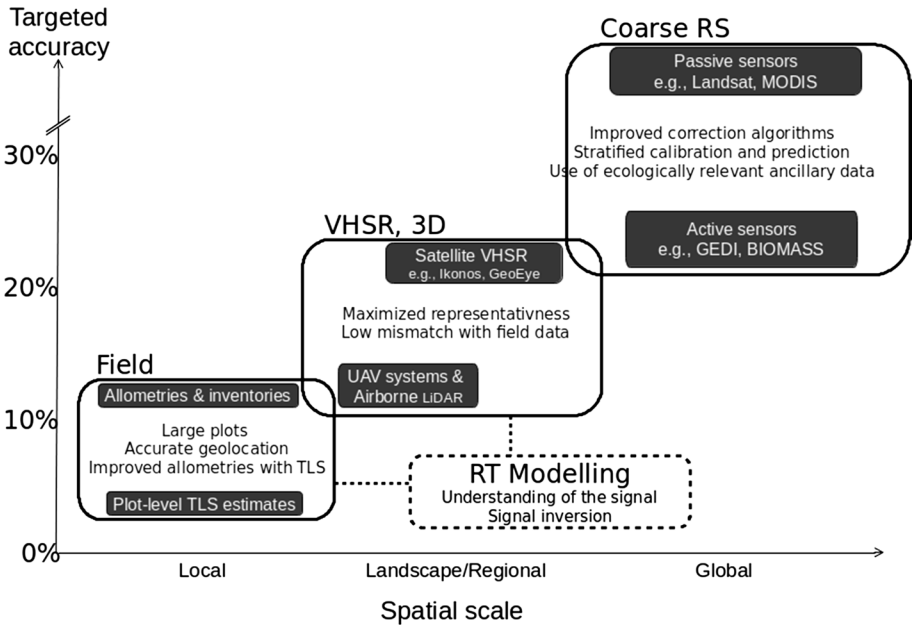

Fig. 9 Best-practice guidelines to upscale AGB estimates from local to global scales. The targeted accuracy (*Y* axis) refers to a 1-ha scale

as the scene is progressively simplified in terms of representation (Jonckheere et al. 2006; Widlowski et al. 2013; Antin et al. 2015).

7 Conclusions and Perspectives

By reviewing the advances and limitations in biomass estimation at each level of the processing chain, we propose a logical workflow that combines what could be considered as best practices given the current state of knowledge (Fig. 9).

Because almost all steps of the processing chain rely on statistical models, the quality of calibration/validation data is crucial, yet often neglected. In this review, we first discussed common-sense procedures to drastically reduce the error levels at the field plot scale, such as improving georeferencing, increasing field plot size (1 ha or more) or developing allometric equations that better account for local ecological variations in plant composition and/or architecture. Terrestrial LiDAR scanning appears to be a promising avenue for individual-level and plot-level measurements of aboveground volumes. Combined with representative WD estimates that account for the intra- and inter-individual patterns of WD variations, robust predictions of AGB may be achievable. Furthermore, the combination of TLS and airborne LiDAR measurements in the upscaling scheme may significantly reduce the source of mismatches described in Sect. 3, allowing for the easy-to-perform control of coregistration and ensuring a continuum in the measured objects (Kükenbrink et al. 2017).

The extrapolation of local estimates to global scales should ideally be performed in successive steps, relying on intermediate, high-resolution data, such as VHSR spaceborne

optical imagery, airborne or UAV-based LiDAR and (UAV-based) stereophotogrammetry. These data can be used to estimate AGB with an accuracy close to the accuracy of ground estimates, but they dramatically increase the representativeness of calibration data when earth observation data of decreased sensitivity (but also decreased cost) are to be used for regional to global predictions. The recent and rapid development of UAV systems, which currently fill the gap between terrestrial and airborne laser scanning systems, is particularly promising because these systems have the potential to bridge different spatial scales, from within-individual-tree to Earth observation pixels of medium resolution (e.g., MODIS).

In parallel, efforts should be expanded to better understand the interactions between different types of electromagnetic signals in varying contexts, e.g., RADAR, LiDAR and passive optical systems, to fully assess the potential of multisensor data fusion. These interactions may be largely blurred by numerous sources of noise and bias—instrumental, atmospheric, geometric, etc. Radiative Transfer (RT) modelling and the prospect to attain a high degree of realism in 3D stand modelling have made this approach a central tool for performing sensitivity analysis and designing signal correction algorithms. Assuming that 3D simulated stands will soon closely reflect reality, they may even be used to directly calibrate inversion models, bypassing many issues such as plot geolocation problems.

The last promise comes from the launch of new space missions (BIOMASS, GEDI, Icesat-2, MOLI, NISAR), which will improve our extrapolation capacities by providing both global coverage and signals of increased relevance. However, whether used individually or in fusion, the calibration of these products should rely on a pre-stratification of forested lands, with enough reference data in each stratum, as it is unlikely that a single universal model can be transferable across forest types and regions without biases.

To conclude, even high-quality Earth observation data currently do not meet the requirements of international environmental policies (e.g., IPCC GPG, REDD+, SDGs, see Herold et al. 2019). Understanding the sources of error and pathways to improve biomass estimation at all levels (as explained in this paper) is fundamental to implementing the best possible practices at each step, resulting in high-quality, consistent biomass estimates with uncertainties quantified to serve the various applications and users.

Acknowledgements We gratefully thank the organizers of the Workshop held at ISSI Bern in November 2017 that was at the origin of this Special Issue. This review has been conducted under the project 3DForMod funded by ERA-GAS (ANR-17-EGAS-0002-01, NWO-3DForMod-5160957540) and has also benefited from the "Investissement d'Avenir" programs managed by Agence Nationale de la Recherche (CEBA, ref. ANR-10-LABX-25-01).

References

Antin C, Grau E, Vincent G et al (2015) From leave scale to tree scale: which structural parameters influence a simulated full-waveform large-footprint LiDAR signal? SilviLaser 2015:110–112

Arciniegas A, Prieto F, Brancheriau L, Lasaygues P (2014) Literature review of acoustic and ultrasonic tomography in standing trees. Trees 28:1559–1567

Asner GP, Mascaro J (2014) Mapping tropical forest carbon: calibrating plot estimates to a simple LiDAR metric. Remote Sens Environ 140:614–624

Asner GP, Broadbent EN, Oliveira PJC et al (2006) Condition and fate of logged forests in the Brazilian Amazon. Proc Natl Acad Sci 103:12947–12950. https://doi.org/10.1073/pnas.0604093103

Asner GP, Mascaro J, Anderson C et al (2013) High-fidelity national carbon mapping for resource management and REDD+. Carbon Balance Manag 8:1–14. https://doi.org/10.1186/1750-0680-8-7

Avitabile V, Camia A (2018) An assessment of forest biomass maps in Europe using harmonized national statistics and inventory plots. For Ecol Manag 409:489–498. https://doi.org/10.1016/j.foreco.2017.11.047
Avitabile V, Herold M, Heuvelink GBM et al (2016) An integrated pan-tropical biomass map using multiple reference datasets. Glob Change Biol 22:1406–1420. https://doi.org/10.1111/gcb.13139
Baccini A, Asner GP (2013) Improving pantropical forest carbon maps with airborne LiDAR sampling. Carbon Manag 4:591–600
Baccini A, Goetz SJ, Walker WS et al (2012) Estimated carbon dioxide emissions from tropical deforestation improved by carbon-density maps. Nat Clim Change 2:182–185. https://doi.org/10.1038/nclimate1354
Baker TR, Phillips OL, Malhi Y et al (2004) Variation in wood density determines spatial patterns in Amazonian forest biomass. Glob Change Biol 10:545–562
Banin L, Feldpausch TR, Phillips OL et al (2012) What controls tropical forest architecture? Testing environmental, structural and floristic drivers. Glob Ecol Biogeogr 21:1179–1190. https://doi.org/10.1111/j.1466-8238.2012.00778.x
Barbier N, Couteron P (2015) Attenuating the bidirectional texture variation of satellite images of tropical forest canopies. Remote Sens Environ 171:245–260
Barbier N, Proisy C, Véga C et al (2011) Bidirectional texture function of high resolution optical images of tropical forest: an approach using LiDAR hillshade simulations. Remote Sens Environ 115:167–179
Bastin J-F, Barbier N, Couteron P et al (2014) Aboveground biomass mapping of African forest mosaics using canopy texture analysis: toward a regional approach. Ecol Appl 24:1984–2001. https://doi.org/10.1890/13-1574.1
Bastin J-F, Fayolle A, Tarelkin Y et al (2015a) Wood specific gravity variations and biomass of central african tree species: the simple choice of the outer wood. PLoS ONE 10:e0142146
Bastin J-F, Barbier N, Réjou-Méchain M et al (2015b) Seeing Central African forests through their largest trees. Sci Rep 5:13156
Bauwens S, Bartholomeus H, Calders K, Lejeune P (2016) Forest inventory with terrestrial LiDAR: a comparison of static and hand-held mobile laser scanning. Forests 7:127
Béland M, Baldocchi DD, Widlowski J-L et al (2014) On seeing the wood from the leaves and the role of voxel size in determining leaf area distribution of forests with terrestrial LiDAR. Agric For Meteorol 184:82–97
Blanchard E, Birnbaum P, Proisy C et al (2015) Prédire la structure des forêts tropicales humides calédoniennes: analyse texturale de la canopée sur des images Pléiades. Rev Fr Photogrammétrie Télédétection 209:141–147
Bouvet A, Mermoz S, Le Toan T et al (2018) An above-ground biomass map of African savannahs and woodlands at 25 m resolution derived from ALOS PALSAR. Remote Sens Environ 206:156–173
Bouvier M, Durrieu S, Fournier RA, Renaud J-P (2015) Generalizing predictive models of forest inventory attributes using an area-based approach with airborne LiDAR data. Remote Sens Environ 156:322–334
Brede B, Lau A, Bartholomeus HM, Kooistra L (2017) Comparing RIEGL RiCOPTER UAV LiDAR derived canopy height and DBH with terrestrial LiDAR. Sensors 17:2371
Bustamante MMC, Roitman I, Aide TM et al (2016) Toward an integrated monitoring framework to assess the effects of tropical forest degradation and recovery on carbon stocks and biodiversity. Glob Change Biol 22:92–109. https://doi.org/10.1111/gcb.13087
Calders K, Newnham G, Burt A et al (2014) Nondestructive estimates of above-ground biomass using terrestrial laser scanning. Methods Ecol Evol. https://doi.org/10.1111/2041-210x.12301
Calders K, Origo N, Burt A et al (2018) Realistic forest stand reconstruction from terrestrial LiDAR for radiative transfer modelling. Remote Sens 10:933
Cescatti A (1997) Modelling the radiative transfer in discontinuous canopies of asymmetric crowns. I. Model structure and algorithms. Ecol Model 101:263–274
Chambers JQ, Negron-Juarez RI, Marra DM et al (2013) The steady-state mosaic of disturbance and succession across an old-growth Central Amazon forest landscape. Proc Natl Acad Sci 110:3949–3954. https://doi.org/10.1073/pnas.1202894110
Chanthorn W, Hartig F, Brockelman WY (2017) Structure and community composition in a tropical forest suggest a change of ecological processes during stand development. For Ecol Manag 404:100–107. https://doi.org/10.1016/j.foreco.2017.08.001
Chave J, Condit R, Aguilar S et al (2004) Error propagation and scaling for tropical forest biomass estimates. Philos Trans R Soc Lond Ser B-Biol Sci 359:409–420
Chave J, Andalo C, Brown S et al (2005) Tree allometry and improved estimation of carbon stocks and balance in tropical forests. Oecologia 145:87–99. https://doi.org/10.1007/s00442-005-0100-x

Chave J, Coomes D, Jansen S et al (2009) Towards a worldwide wood economics spectrum. Ecol Lett 12:351–366
Chave J, Réjou-Méchain M, Búrquez A et al (2014) Improved allometric models to estimate the aboveground biomass of tropical trees. Glob Change Biol 20:3177–3190. https://doi.org/10.1111/gcb.12629
Chen Q, Laurin GV, Valentini R (2015) Uncertainty of remotely sensed aboveground biomass over an African tropical forest: propagating errors from trees to plots to pixels. Remote Sens Environ 160:134–143
Clark DA (2002) Are tropical forests an important carbon sink? Reanalysis of the long-term plot data. Ecol Appl 12:3–7. https://doi.org/10.1890/1051-0761(2002)012%5b0003:atfaic%5d2.0.co;2
Clark D, Clark D (2000) Landscape-scale variation in forest structure and biomass in a tropical rain forest. For Ecol Manag 137:185–198. https://doi.org/10.1016/s0378-1127(99)00327-8
Clark DB, Kellner JR (2012) Tropical forest biomass estimation and the fallacy of misplaced concreteness. J Veg Sci 23:1191–1196. https://doi.org/10.1111/j.1654-1103.2012.01471.x
Condit R (1998) Tropical forest census plots: methods and results from Barro Colorado Island, Panama and a comparison with other plots. Springer, Berlin
Condit R, Ashton PS, Baker P et al (2000) Spatial patterns in the distribution of tropical tree species. Science 288(5470):1414–1418
Condit R, Lao S, Singh A et al (2014) Data and database standards for permanent forest plots in a global network. For Ecol Manag 316:21–31
Côté J-F, Fournier RA, Egli R (2011) An architectural model of trees to estimate forest structural attributes using terrestrial LiDAR. Environ Model Softw 26:761–777. https://doi.org/10.1016/j.envsoft.2010.12.008
Couteron P, Pelissier R, Nicolini EA, Paget D (2005) Predicting tropical forest stand structure parameters from Fourier transform of very high-resolution remotely sensed canopy images. J Appl Ecol 42:1121–1128
Dauzat J, Rapidel B, Berger A (2001) Simulation of leaf transpiration and sap flow in virtual plants: model description and application to a coffee plantation in Costa Rica. Agric For Meteorol 109:143–160
de Castilho CV, Magnusson WE, de Araújo RNO et al (2006) Variation in aboveground tree live biomass in a central Amazonian forest: effects of soil and topography. For Ecol Manag 234:85–96. https://doi.org/10.1016/j.foreco.2006.06.024
de Moura YM, Hilker T, Goncalves FG et al (2016) Scaling estimates of vegetation structure in Amazonian tropical forests using multi-angle MODIS observations. Int J Appl Earth Obs Geoinf 52:580–590
De Reffye P, Houllier F, Blaise F et al (1995) A model simulating above-and below-ground tree architecture with agroforestry applications. Agrofor Syst 30:175–197
de Souza Pereira FR, Kampel M, Gomes Soares ML et al (2018) Reducing uncertainty in mapping of mangrove aboveground biomass using airborne discrete return LiDAR data. Remote Sens 10:637
Detto M, Muller-Landau HC, Mascaro J, Asner GP (2013) Hydrological networks and associated topographic variation as templates for the spatial organization of tropical forest vegetation. PLoS ONE 8:e76296. https://doi.org/10.1371/journal.pone.0076296
Dickinson TA, Tanner EVJ (1978) Exploitation of hollow trunks by tropical trees. Biotropica 10:231–233. https://doi.org/10.2307/2387908
Disney M (2018) Terrestrial LiDAR: a 3D revolution in how we look at trees. New Phytol. https://doi.org/10.1111/nph.15517
Egbert DD (1977) A practical method for correcting bidirectional reflectance variations. In: LARS symposia, p 203
Emilio T, Quesada CA, Costa FRC et al (2013) Soil physical conditions limit palm and tree basal area in Amazonian forests. Plant Ecol Divers 10:1. https://doi.org/10.1080/17550874.2013.772257
ESA (2012) Report for mission selection: biomass, ESA SP-1324/1 (3 volume series). European Space Agency Noordwijk, The Netherlands
Fayad I, Baghdadi N, Guitet S et al (2016) Aboveground biomass mapping in French Guiana by combining remote sensing, forest inventories and environmental data. Int J Appl Earth Obs Geoinf 52:502–514
Fayolle A, Doucet J-L, Gillet J-F et al (2013) Tree allometry in Central Africa: testing the validity of pantropical multi-species allometric equations for estimating biomass and carbon stocks. For Ecol Manag 305:29–37. https://doi.org/10.1016/j.foreco.2013.05.036
Feldpausch TR, Banin L, Phillips OL et al (2011) Height–diameter allometry of tropical forest trees. Biogeosciences 8:1081–1106
Feldpausch TR, Lloyd J, Lewis SL et al (2012) Tree height integrated into pantropical forest biomass estimates. Biogeosciences 9:3381–3403. https://doi.org/10.5194/bg-9-3381-2012
Féret J-B, Asner GP (2014) Mapping tropical forest canopy diversity using high-fidelity imaging spectroscopy. Ecol Appl 24:1289–1296

Ferraz A, Saatchi S, Mallet C, Meyer V (2016) LiDAR detection of individual tree size in tropical forests. Remote Sens Environ 183:318–333
Féret JB, Gitelson AA, Noble SD, Jacquemoud S (2017) PROSPECT-D: towards modeling leaf optical properties through a complete lifecycle. Remote Sens Environ 193:204–215
Flores O, Coomes DA (2011) Estimating the wood density of species for carbon stock assessments. Methods Ecol Evol 2:214–220. https://doi.org/10.1111/j.2041-210x.2010.00068.x
Frazer GW, Wulder MA, Niemann KO (2005) Simulation and quantification of the fine-scale spatial pattern and heterogeneity of forest canopy structure: a lacunarity-based method designed for analysis of continuous canopy heights. For Ecol Manag 214:65–90
Frazer GW, Magnussen S, Wulder MA, Niemann KO (2011) Simulated impact of sample plot size and co-registration error on the accuracy and uncertainty of LiDAR-derived estimates of forest stand biomass. Remote Sens Environ 115:636–649
Fuller WA (1987) Measurement error models. Wiley, New York
Gao S, Wang X, Wiemann MC et al (2017) A critical analysis of methods for rapid and nondestructive determination of wood density in standing trees. Ann For Sci 74:27
Gastellu-Etchegorry J-P, Demarez V, Pinel V, Zagolski F (1996) Modeling radiative transfer in heterogeneous 3-D vegetation canopies. Remote Sens Environ 58:131–156
Gastellu-Etchegorry J-P, Yin T, Lauret N et al (2015) Discrete anisotropic radiative transfer (DART 5) for modeling airborne and satellite spectroradiometer and LiDAR acquisitions of natural and urban landscapes. Remote Sens 7:1667–1701
Gobakken T, Naesset E (2009) Assessing effects of positioning errors and sample plot size on biophysical stand properties derived from airborne laser scanner data. Can J For Res 39:1036–1052
Gomes ACS, Andrade A, Barreto-Silva JS et al (2013) Local plant species delimitation in a highly diverse Amazonian forest: do we all see the same species? J Veg Sci 24:70–79. https://doi.org/10.1111/j.1654-1103.2012.01441.x
Gonzalez de Tanago J, Lau A, Bartholomeus H et al (2018) Estimation of above-ground biomass of large tropical trees with terrestrial LiDAR. Methods Ecol Evol 9:223–234
Goodman RC, Phillips OL, Baker TR (2014) The importance of crown dimensions to improve tropical tree biomass estimates. Ecol Appl 24:680–698. https://doi.org/10.1890/13-0070.1
Gourlet-Fleury S, Rossi V, Réjou-Méchain M et al (2011) Environmental filtering of dense-wooded species controls above-ground biomass stored in African moist forests. J Ecol 99:981–990. https://doi.org/10.1111/j.1365-2745.2011.01829.x
Grau E, Durrieu S, Fournier R et al (2017) Estimation of 3D vegetation density with terrestrial laser scanning data using voxels. A sensitivity analysis of influencing parameters. Remote Sens Environ 191:373–388
Gregoire TG, Næsset E, McRoberts RE et al (2016) Statistical rigor in LiDAR-assisted estimation of aboveground forest biomass. Remote Sens Environ 173:98–108
Guitet S, Pélissier R, Brunaux O et al (2015) Geomorphological landscape features explain floristic patterns in French Guiana rainforest. Biodivers Conserv 24:1215–1237
Guitet S, Sabatier D, Brunaux O et al (2018) Disturbance regimes drive the diversity of regional floristic pools across Guianan rainforest landscapes. Sci Rep 8:3872
Hajj ME, Baghdadi N, Fayad I et al (2017) Interest of integrating spaceborne LiDAR data to improve the estimation of biomass in high biomass forested areas. Remote Sens 9:213
Hansen MC, Potapov PV, Moore R et al (2013) High-resolution global maps of 21st-century forest cover change. Science 342:850–853
Henry M, Besnard A, Asante WA et al (2010) Wood density, phytomass variations within and among trees, and allometric equations in a tropical rainforest of Africa. For Ecol Manag 260:1375–1388
Herold M, Carter S, Avitabile V et al (2019) The role and need for space-based forest biomass-related measurements in environmental management and policy. Surv Geophys. https://doi.org/10.1007/s10712-019-09510-6
Huang W, Swatantran A, Johnson K et al (2015) Local discrepancies in continental scale biomass maps: a case study over forested and non-forested landscapes in Maryland, USA. Carbon Balance Manag 10:19
Hunter MO, Keller M, Victoria D, Morton DC (2013) Tree height and tropical forest biomass estimation. Biogeosciences 10:8385–8399
Inglada J, Vadon H (2005) Fine registration of SPOT5 and Envisat/ASAR images and ortho-image production: a fully automatic approach. In: Proceedings 2005 IEEE international geoscience and remote sensing symposium, 2005. IGARSS'05. IEEE, Vol. 5, pp 3510–3512
Ishimaru A (1978) Wave propagation and scattering in random media, vol 2. Academic press, New York, pp 336–393

Johnson CE, Barton CC (2004) Where in the world are my field plots? Using GPS effectively in environmental field studies. Front Ecol Environ 2:475–482. https://doi.org/10.1890/1540-9295(2004)002%5b0475:witwam%5d2.0.co;2
Jonckheere I, Nackaerts K, Muys B et al (2006) A fractal dimension-based modelling approach for studying the effect of leaf distribution on LAI retrieval in forest canopies. Ecol Model 197:179–195
Jucker T, Asner GP, Dalponte M et al (2017a) A regional model for estimating the aboveground carbon density of Borneo's tropical forests from airborne laser scanning. arXiv Prepr arXiv170509242
Jucker T, Caspersen J, Chave J et al (2017b) Allometric equations for integrating remote sensing imagery into forest monitoring programmes. Glob Change Biol 23:177–190
Jucker T, Asner GP, Dalponte M et al (2018a) Estimating aboveground carbon density and its uncertainty in Borneo's structurally complex tropical forests using airborne laser scanning. Biogeosciences 15:3811–3830
Jucker T, Bongalov B, Burslem DF et al (2018b) Topography shapes the structure, composition and function of tropical forest landscapes. Ecol Lett 21:989–1000
Justice CO, Giglio L, Korontzi S et al (2002) The MODIS fire products. Remote Sens Environ 83:244–262
Kearsley E, De Haulleville T, Hufkens K et al (2013) Conventional tree height–diameter relationships significantly overestimate aboveground carbon stocks in the Central Congo Basin. Nat Commun 4:2269
Kellner JR, Asner GP (2009) Convergent structural responses of tropical forests to diverse disturbance regimes. Ecol Lett 12:887–897
Kennedy RE, Yang Z, Cohen WB (2010) Detecting trends in forest disturbance and recovery using yearly Landsat time series: 1. LandTrendr—temporal segmentation algorithms. Remote Sens Environ 114:2897–2910
Ketterings QM, Coe R, van Noordwijk M et al (2001) Reducing uncertainty in the use of allometric biomass equations for predicting above-ground tree biomass in mixed secondary forests. For Ecol Manag 146:199–209. https://doi.org/10.1016/s0378-1127(00)00460-6
Kleinn C (2017) The renaissance of National Forest Inventories (NFIs) in the context of the international conventions—a discussion paper on context, background and justification of NFIs. Pesqui Florest Bras 37:369–379
Kükenbrink D, Schneider FD, Leiterer R et al (2017) Quantification of hidden canopy volume of airborne laser scanning data using a voxel traversal algorithm. Remote Sens Environ 194:424–436. https://doi.org/10.1016/j.rse.2016.10.023
Labriere N, Tao S, Chave J et al (2018) In situ reference datasets from the TropiSAR and AfriSAR campaigns in support of upcoming spaceborne biomass missions. IEEE J Sel Top Appl Earth Obs Remote Sens 99:1–11
Lagomasino D, Fatoyinbo T, Lee S-K, Simard M (2015) High-resolution forest canopy height estimation in an African blue carbon ecosystem. Remote Sens Ecol Conserv 1:51–60. https://doi.org/10.1002/rse2.3
Larjavaara M, Muller-Landau HC (2013) Measuring tree height: a quantitative comparison of two common field methods in a moist tropical forest. Methods Ecol Evol 4:793–801. https://doi.org/10.1111/2041-210x.12071
Lau A, Bentley LP, Martius C et al (2018) Quantifying branch architecture of tropical trees using terrestrial LiDAR and 3D modelling. Trees 32(5):1219–1231
Le Toan T, Quegan S, Davidson MWJ et al (2011) The BIOMASS mission: mapping global forest biomass to better understand the terrestrial carbon cycle. Remote Sens Environ 115:2850–2860. https://doi.org/10.1016/j.rse.2011.03.020
Lefsky MA, Cohen WB, Parker GG, Harding DJ (2002) LiDAR remote sensing for ecosystem studies LiDAR, an emerging remote sensing technology that directly measures the three-dimensional distribution of plant canopies, can accurately estimate vegetation structural attributes and should be of particular interest to forest, landscape, and global ecologists. Bioscience 52:19–30
Leitold V, Morton DC, Longo M et al (2018) El Niño drought increased canopy turnover in Amazon forests. New Phytol 219:959–971
Li X, Strahler AH (1992) Geometric-optical bidirectional reflectance modeling of the discrete crown vegetation canopy: effect of crown shape and mutual shadowing. IEEE Trans Geosci Remote Sens 30:276–292
Lindenmayer DB, Cunningham RB, Tanton MT et al (1991) Characteristics of hollow-bearing trees occupied by arboreal marsupials in the montane ash forests of the Central Highlands of Victoria, southeast Australia. For Ecol Manag 40:289–308
Liu J-Y, Zheng Z, Xu X et al (2018) Abundance and distribution of cavity trees and the effect of topography on cavity presence in a tropical rainforest, southwestern China. Can J For Res 48:1058–1066

Longo M, Keller M, dos-Santos MN et al (2016) Aboveground biomass variability across intact and degraded forests in the Brazilian Amazon. Glob Biogeochem Cycles 30:1639–1660
Lopez-Gonzalez G, Lewis SL, Burkitt M, Phillips OL (2011) ForestPlots.net: a web application and research tool to manage and analyse tropical forest plot data. J Veg Sci 22:610–613
Lyapustin A, Martonchik J, Wang Y et al (2011) Multiangle implementation of atmospheric correction (MAIAC): 1. Radiative transfer basis and look-up tables. J Geophys Res Atmos 116:1–9
Ma L, Zheng G, Eitel JU et al (2016) Improved salient feature-based approach for automatically separating photosynthetic and nonphotosynthetic components within terrestrial LiDAR point cloud data of forest canopies. IEEE Trans Geosci Remote Sens 54:679–696
Malenovskỳ Z, Martin E, Homolová L et al (2008) Influence of woody elements of a Norway spruce canopy on nadir reflectance simulated by the DART model at very high spatial resolution. Remote Sens Environ 112:1–18
Marra RE, Brazee NJ, Fraver S (2018) Estimating carbon loss due to internal decay in living trees using tomography: implications for forest carbon budgets. Environ Res Lett. https://doi.org/10.1088/1748-9326/aae2bf
Marvin DC, Asner GP, Knapp DE et al (2014) Amazonian landscapes and the bias in field studies of forest structure and biomass. Proc Natl Acad Sci 111:E5224–E5232. https://doi.org/10.1073/pnas.1412999111
Mascaro J, Detto M, Asner GP, Muller-Landau HC (2011) Evaluating uncertainty in mapping forest carbon with airborne LiDAR. Remote Sens Environ 115:3770–3774. https://doi.org/10.1016/j.rse.2011.07.019
McEwan RW, Lin Y-C, Sun I-F et al (2011) Topographic and biotic regulation of aboveground carbon storage in subtropical broad-leaved forests of Taiwan. For Ecol Manag 262:1817–1825. https://doi.org/10.1016/j.foreco.2011.07.028
McRoberts RE, Westfall JA (2013) Effects of uncertainty in model predictions of individual tree volume on large area volume estimates. For Sci 60(1):34–42
Mermoz S, Le Toan T, Villard L et al (2014) Biomass assessment in the Cameroon savanna using ALOS PALSAR data. Remote Sens Environ 155:109–119. https://doi.org/10.1016/j.rse.2014.01.029
Mermoz S, Réjou-Méchain M, Villard L et al (2015) Decrease of L-band SAR backscatter with biomass of dense forests. Remote Sens Environ 15:307–317. https://doi.org/10.1016/j.rse.2014.12.019
Minh DHT, Le Toan T, Rocca F et al (2014) Relating P-band synthetic aperture radar tomography to tropical forest biomass. IEEE Trans Geosci Remote Sens 52:967–979
Minh DHT, Le Toan T, Rocca F et al (2016) SAR tomography for the retrieval of forest biomass and height: cross-validation at two tropical forest sites in French Guiana. Remote Sens Environ 175:138–147
Mitchard ETA (2018) The tropical forest carbon cycle and climate change. Nature 559:527–534. https://doi.org/10.1038/s41586-018-0300-2
Mitchard ET, Saatchi SS, Baccini A et al (2013) Uncertainty in the spatial distribution of tropical forest biomass: a comparison of pan-tropical maps. Carbon Balance Manage 8:10
Mitchard ETA, Feldpausch TR, Brienen RJW et al (2014) Markedly divergent estimates of Amazon forest carbon density from ground plots and satellites. Glob Ecol Biogeogr 23:935–946. https://doi.org/10.1111/geb.12168
Molto Q, Rossi V, Blanc L (2013) Error propagation in biomass estimation in tropical forests. Methods Ecol Evol 4:175–183. https://doi.org/10.1111/j.2041-210x.2012.00266.x
Momo Takoudjou S, Ploton P, Sonké B et al (2018) Using terrestrial laser scanning data to estimate large tropical trees biomass and calibrate allometric models: a comparison with traditional destructive approach. Methods Ecol Evol 9:905–916
Morsdorf F, Eck C, Zgraggen C et al (2017) UAV-based LiDAR acquisition for the derivation of high-resolution forest and ground information. Lead Edge 36:566–570
Morton DC, Nagol J, Carabajal CC et al (2014) Amazon forests maintain consistent canopy structure and greenness during the dry season. Nature 506:221–224. https://doi.org/10.1038/nature13006
Moundounga Mavouroulou Q, Ngomanda A, Engone Obiang NL et al (2014) How to improve allometric equations to estimate forest biomass stocks? Some hints from a central African forest. Can J For Res 44:685–691
Myneni RB (1991) Modeling radiative transfer and photosynthesis in three-dimensional vegetation canopies. Agric For Meteorol 55:323–344
Myneni RB, Ross J, Asrar G (1989) A review on the theory of photon transport in leaf canopies. Agric For Meteorol 45:1–153
Ni W, Li X, Woodcock CE et al (1999) An analytical hybrid GORT model for bidirectional reflectance over discontinuous plant canopies. IEEE Trans Geosci Remote Sens 37:987–999

Nogueira EM, Nelson BW, Fearnside PM (2006) Volume and biomass of trees in central Amazonia: influence of irregularly shaped and hollow trunks. For Ecol Manag 227:14–21. https://doi.org/10.1016/j.foreco.2006.02.004
North PR (1996) Three-dimensional forest light interaction model using a Monte Carlo method. IEEE Trans Geosci Remote Sens 34:946–956
Pargal S, Fararoda R, Rajashekar G et al (2017) Inverting aboveground biomass–canopy texture relationships in a landscape of Forest mosaic in the Western Ghats of India using very high resolution Cartosat imagery. Remote Sens 9:228
Pearson TR, Brown S, Murray L, Sidman G (2017) Greenhouse gas emissions from tropical forest degradation: an underestimated source. Carbon Balance Manag 12:3
Phillips OL, Baker TR, Brienen R, Feldpausch TR (2009) Field manual for plot establishment and remeasurement. https://www.forestplots.net/upload/ManualsEnglish/RAINFOR_field_manual_EN.pdf
Ploton P, Pélissier R, Proisy C et al (2012) Assessing aboveground tropical forest biomass using Google Earth canopy images. Ecol Appl 22:993–1003
Ploton P, Pélissier R, Barbier N et al (2013) Canopy texture analysis for large-scale assessments of tropical forest stand structure and biomass. In: Devy S, Ganesh T, Lowman MD (eds) Treetops at risk. Springer, Berlin, pp 237–245
Ploton P, Barbier N, Momo ST et al (2016) Closing a gap in tropical forest biomass estimation: taking crown mass variation into account in pantropical allometries. Biogeosciences 13:1571–1585
Ploton P, Barbier N, Couteron P et al (2017) Toward a general tropical forest biomass prediction model from very high resolution optical satellite images. Remote Sens Environ 200:140–153
Proisy C, Couteron P, Fromard F (2007) Predicting and mapping mangrove biomass from canopy grain analysis using Fourier-based textural ordination of IKONOS images. Remote Sens Environ 109:379–392. https://doi.org/10.1016/j.rse.2007.01.009
Puliti S, Ørka HO, Gobakken T, Næsset E (2015) Inventory of small forest areas using an unmanned aerial system. Remote Sens 7:9632–9654
Raumonen P, Kaasalainen M, Åkerblom M et al (2013) Fast automatic precision tree models from terrestrial laser scanner data. Remote Sens 5:491–520
Réjou-Méchain M, Muller-Landau HC, Detto M et al (2014) Local spatial structure of forest biomass and its consequences for remote sensing of carbon stocks. Biogeosciences 11:6827–6840
Réjou-Méchain M, Tymen B, Blanc L et al (2015) Using repeated small-footprint LiDAR maps to infer spatial variation and dynamics of a high-biomass neotropical forest. Remote Sens Environ 169:93–101
Réjou-Méchain M, Tanguy A, Piponiot C et al (2017) BIOMASS: an r package for estimating above-ground biomass and its uncertainty in tropical forests. Methods Ecol Evol 8:1163–1167
Robinson C, Saatchi S, Neumann M, Gillespie T (2013) Impacts of spatial variability on aboveground biomass estimation from L-band radar in a temperate forest. Remote Sens 5:1001–1023
Rocchini D, Luque S, Pettorelli N et al (2018) Measuring β-diversity by remote sensing: a challenge for biodiversity monitoring. Methods Ecol Evol 9:1787–1798
Rodrigues WA, Valle RC (1964) Ocorrência de troncos ocos em mata de baixio da regiao de Manaus, 16th edn. Publicacao. Botanica - Instituto Nacional de Pesquisa da Amazonia (Brazil), Manaus
Rodriguez-Veiga P, Wheeler J, Louis V et al (2017) Quantifying forest biomass carbon stocks from space. Curr For Rep 3:1–18
Romijn E, De Sy V, Herold M et al (2018) Independent data for transparent monitoring of greenhouse gas emissions from the land use sector—what do stakeholders think and need? Environ Sci Policy 85:101–112
Roşca S, Suomalainen J, Bartholomeus H, Herold M (2018) Comparing terrestrial laser scanning and unmanned aerial vehicle structure from motion to assess top of canopy structure in tropical forests. Interface Focus 8:20170038
Rosen P, Hensley S, Shaffer S et al (2017) The NASA-ISRO SAR (NISAR) mission dual-band radar instrument preliminary design. In: 2017 IEEE international geoscience and remote sensing symposium (IGARSS), pp 3832–3835
Roujean J-L, Leroy M, Deschamps P-Y (1992) A bidirectional reflectance model of the Earth's surface for the correction of remote sensing data. J Geophys Res Atmos 97:20455–20468
Saatchi SS, Houghton RA, Alvalá DS et al (2007) Distribution of aboveground live biomass in the Amazon basin. Glob Change Biol 13:816–837. https://doi.org/10.1111/j.1365-2486.2007.01323.x
Saatchi S, Marlier M, Chazdon RL et al (2011a) Impact of spatial variability of tropical forest structure on radar estimation of aboveground biomass. Remote Sens Environ 115:2836–2849. https://doi.org/10.1016/j.rse.2010.07.015

Saatchi SS, Harris NL, Brown S et al (2011b) Benchmark map of forest carbon stocks in tropical regions across three continents. Proc Natl Acad Sci 108:9899–9904. https://doi.org/10.1073/pnas.1019576108

Saatchi S, Mascaro J, Xu L et al (2015) Seeing the forest beyond the trees. Glob Ecol Biogeogr 24:606–610

Sagang LBT, Momo ST, Libalah MB et al (2018) Using volume-weighted average wood specific gravity of trees reduces bias in aboveground biomass predictions from forest volume data. For Ecol Manag 424:519–528. https://doi.org/10.1016/j.foreco.2018.04.054

Santoro M, Cartus O, Mermoz S et al (2018) A detailed portrait of the forest aboveground biomass pool for the year 2010 obtained from multiple remote sensing observations. In: EGU general assembly conference abstracts, p 18932

Schlund M, von Poncet F, Kuntz S et al (2015) TanDEM-X data for aboveground biomass retrieval in a tropical peat swamp forest. Remote Sens Environ 158:255–266

Schneider FD, Yin T, Gastellu-Etchegorry J et al (2014) At-sensor radiance simulation for airborne imaging spectroscopy. In: 2014 6th workshop on hyperspectral image and signal processing: evolution in remote sensing (WHISPERS), pp 1–4

Sigrist P, Coppin P, Hermy M (1999) Impact of forest canopy on quality and accuracy of GPS measurements. Int J Remote Sens 20:3595–3610. https://doi.org/10.1080/014311699211228

Simard M, Pinto N, Fisher JB, Baccini A (2011) Mapping forest canopy height globally with spaceborne LiDAR. J Geophys Res Biogeosci 116:1–12

Singh M, Malhi Y, Bhagwat S (2014) Biomass estimation of mixed forest landscape using a Fourier transform texture-based approach on very-high-resolution optical satellite imagery. Int J Remote Sens 35:3331–3349

Sitch S, Huntingford C, Gedney N et al (2008) Evaluation of the terrestrial carbon cycle, future plant geography and climate-carbon cycle feedbacks using five dynamic global vegetation models (DGVMs). Glob Change Biol 14:2015–2039

Solberg S, May J, Bogren W et al (2018) Interferometric SAR DEMs for forest change in Uganda 2000–2012. Remote Sens 10:228

Steininger MK (2000) Satellite estimation of tropical secondary forest above-ground biomass: data from Brazil and Bolivia. Int J Remote Sens 21:1139–1157

St-Onge B, Vega C, Fournier RA, Hu Y (2008) Mapping canopy height using a combination of digital stereo-photogrammetry and LiDAR. Int J Remote Sens 29:3343–3364

Sullivan MJ, Lewis SL, Hubau W et al (2018) Field methods for sampling tree height for tropical forest biomass estimation. Methods Ecol Evol 9:1179–1189

Sun G, Ranson KJ (2000) Modeling LiDAR returns from forest canopies. IEEE Trans Geosci Remote Sens 38:2617–2626

Swenson NG, Enquist BJ (2008) The relationship between stem and branch wood specific gravity and the ability of each measure to predict leaf area. Am J Bot 95:516–519

Tarelkin Y, Hufkens K, Hahn S et al (2019) Wood anatomy variability under contrasted environmental conditions of common deciduous and evergreen species from central African forests. Trees Struct Funct 33:893–909. https://doi.org/10.1007/s00468-019-01826-5

Trochta J, Krůček M, Vrška T, Král K (2017) 3D Forest: an application for descriptions of three-dimensional forest structures using terrestrial LiDAR. PLoS ONE 12:e0176871

Tymen B, Vincent G, Courtois EA et al (2017) Quantifying micro-environmental variation in tropical rainforest understory at landscape scale by combining airborne LiDAR scanning and a sensor network. Ann For Sci 74:32

Verhoef W (1985) Earth observation modeling based on layer scattering matrices. Remote Sens Environ 17:165–178

Vieilledent G, Vaudry R, Andriamanohisoa SF et al (2012) A universal approach to estimate biomass and carbon stock in tropical forests using generic allometric models. Ecol Appl 22:572–583

Villard L (2009) Forward and inverse modeling of synthetic aperture radar in the bistatic configuration: applications in forest remote sensing. Ph.D. thesis, ONERAISAE-Universite Paul Sabatier

Villard L, Le Toan T (2015) Relating P-band SAR intensity to biomass for tropical dense forests in hilly terrain: γ^0 or t^0? IEEE J Sel Top Appl Earth Obs Remote Sens 8:214–223

Vincent G, Caron F, Sabatier D, Blanc L (2012a) LiDAR shows that higher forests have more slender trees. Bois For Trop 314:51–56

Vincent G, Sabatier D, Blanc L et al (2012b) Accuracy of small footprint airborne LiDAR in its predictions of tropical moist forest stand structure. Remote Sens Environ 125:23–33. https://doi.org/10.1016/j.rse.2012.06.019

Vincent G, Sabatier D, Rutishauser E (2014) Revisiting a universal airborne light detection and ranging approach for tropical forest carbon mapping: scaling-up from tree to stand to landscape. Oecologia 175:439–443

Vincent G, Antin C, Laurans M et al (2017) Mapping plant area index of tropical evergreen forest by airborne laser scanning. A cross-validation study using LAI2200 optical sensor. Remote Sens Environ 198:254–266

Wassenberg M, Chiu H-S, Guo W, Spiecker H (2015) Analysis of wood density profiles of tree stems: incorporating vertical variations to optimize wood sampling strategies for density and biomass estimations. Trees 29:551–561

Widlowski J-L, Pinty B, Lopatka M et al (2013) The fourth radiation transfer model intercomparison (RAMI-IV): proficiency testing of canopy reflectance models with ISO-13528. J Geophys Res Atmos 118:6869–6890. https://doi.org/10.1002/jgrd.50497

Williamson GB, Wiemann MC (2010) Measuring wood specific gravity… correctly. Am J Bot 97:519–524

Wu X, Liu H, Li X et al (2018) Differentiating drought legacy effects on vegetation growth over the temperate Northern Hemisphere. Glob Change Biol 24:504–516

Xu L, Saatchi SS, Yang Y et al (2016) Performance of non-parametric algorithms for spatial mapping of tropical forest structure. Carbon Balance Manag 11:18

Xu L, Saatchi SS, Shapiro A et al (2017) Spatial distribution of carbon stored in forests of the Democratic Republic of Congo. Sci Rep 7:15030

Zanne AE, Lopez-Gonzalez G, Coomes DA, Ilic J, Jansen S, Lewis SL, Miller RB, Swenson NG, Wiemann MC, Chave J (2009) Data from: towards a worldwide wood economics spectrum. Dryad Digit Repos. https://doi.org/10.5061/dryad.234

Zolkos SG, Goetz SJ, Dubayah R (2013) A meta-analysis of terrestrial aboveground biomass estimation using LiDAR remote sensing. Remote Sens Environ 128:289–298. https://doi.org/10.1016/j.rse.2012.10.017

Affiliations

Maxime Réjou-Méchain[1] · Nicolas Barbier[1] · Pierre Couteron[1] · Pierre Ploton[1] · Grégoire Vincent[1] · Martin Herold[2] · Stéphane Mermoz[3,8] · Sassan Saatchi[4] · Jérôme Chave[5] · Florian de Boissieu[6] · Jean-Baptiste Féret[6] · Stéphane Momo Takoudjou[1,7] · Raphaël Pélissier[1]

[1] AMAP, IRD, CNRS, CIRAD, INRA, Univ Montpellier, Montpellier Cedex 05, France

[2] Laboratory of Geo-Information Science and Remote Sensing, Wageningen University and Research, Droevendaalsesteeg 3, 6708 PB Wageningen, The Netherlands

[3] CESBIO, CNES/CNRS, IRD/UPS, Université de Toulouse, Toulouse, France

[4] Jet Propulsion Laboratory, California Institute of Technology, Pasadena, CA 91109, USA

[5] CNRS, ENFA; UMR5174 EDB (Laboratoire Evolution et Diversité Biologique), Université Paul Sabatier, 118 Route de Narbonne, 31062 Toulouse, France

[6] TETIS, Irstea, AgroParisTech, CIRAD, CNRS, University of Montpellier, 34000 Montpellier, France

[7] Plant Systematic and Ecology Laboratory, Higher Teacher's Training College, University of Yaoundé I, P.O. Box 047, Yaoundé, Cameroon

[8] GlobEO, Avenue Saint-Exupery, Toulouse, France